Electron–photon showers produced by gamma quanta and electrons in dense amorphous media

B. Słowiński
Physics Institute, Warsaw Technical University, Poland

Fiz. Elem. Chastits At. Yadra **25**, 417–495 (March–April 1994)

The results from experimental studies of electron–photon showers produced in heavy amorphous media by gamma quanta and electrons with energy in the range from 100 MeV to 200 MeV are reviewed. The basic information about the elementary physical processes comprising a shower is given. The results of cascade theory and numerical modeling of the process by the Monte Carlo method are briefly surveyed. The studies carried out using the ITEP (Moscow) xenon bubble chamber are described in more detail. These provided original experimental data on the longitudinal and transverse shower profiles, as well as on the fluctuations and correlations in showers produced in liquid xenon by gamma quanta of energy 100–3500 MeV. A phenomenological scaling description, obtained from analysis of the experimental data, of the longitudinal and transverse profiles and also of their fluctuations is presented in the form of simple expressions convenient for practical use.

1. INTRODUCTION

In the electric field of a nucleus of an atom in a medium, a high-energy gamma quantum ($E_\gamma \gg 2m_e c^2$, where m_e is the electron rest mass) is converted into an electron–positron pair. In turn, each of the particles of this pair, undergoing acceleration in the Coulomb field of the atomic nuclei of the material, can emit hard gamma quanta (henceforth referred to as photons), which can produce electron–positron pairs, and so on. Therefore, with increasing depth of the medium along the direction of motion of the primary gamma quantum there occurs a multiplication of particles: gamma quanta, electrons, and positrons. This process, referred to as an electron–photon shower (EPS),[1)] develops as long as the energy of the bremsstrahlung gamma quanta exceeds $2m_e c^2$. Then the shower damps out. An EPS can also be produced by an electron, a positron, or, with considerably lower probability, a muon or heavier particle.

Of course, the process of EPS generation is not as simple as this summary of its main features suggests. A significant role is played by ionization and excitation of the atoms of the medium, which are the main factors associated with bremsstrahlung, and also by multiple Coulomb scattering of shower electrons and positrons and Compton scattering of soft gamma quanta, which leads to the three-dimensional structure of the EPS. There are also other phenomena of electromagnetic nature which, in addition, are widely used to detect this phenomenon, in particular, Čerenkov radiation, which also is a bremsstrahlung factor.

Qualitatively new effects arise at energies of 100 GeV and above which noticeably affect the absorption of shower particles in the interior of the medium: the Chudakov effect and the phenomenon first mentioned by Landau and Pomeranchuk, and then analyzed quantitatively at the quantum mechanical level by Migdal (below we refer to this as the LPM effect). These effects lead to an additional increase of primarily the longitudinal dimensions of showers generated by photons (or electrons and positrons) of superhigh energy which develop in dense media. In addition, at energies of several TeV the cross sections for weak and electromagnetic interactions become comparable in magnitude, so that the EPS is enriched by hadrons, muons, and neutrinos, which again mainly tends to increase the longitudinal dimensions of the shower. Finally, when a shower develops in a single crystal and the particle initiating it (a photon, electron, or positron) travels parallel to the crystal axis, the coherence of the bremsstrahlung emission and electron–positron pair production processes can cause the energy loss of the shower particles to increase by an order of magnitude compared to the case of an amorphous medium. As a result of this so-called radiation cooling the longitudinal dimensions of the shower become much smaller, at least in its initial part, where the condition of channeling of the shower particles in the crystal is preserved.

EPS production was first discovered by Rossi in 1932 (Ref. 1). The experimental setup consisted of three Geiger–Mueller counters arranged in the form of a triangle such that they were not triggered simultaneously by a single cosmic-ray ionizing particle. Nevertheless, (35.5 ± 1) coincidences were recorded during one hour. When he then removed the upper part of the lead screen, Rossi noticed a decrease in the number of coincidences to (10.0 ± 0.5) per hour. He attributed this observation to the generation by cosmic rays of secondary ionizing particles in the lead screen (see also p. 372 of Ref. 2). This experiment initiated intensive research, first experimental and then theoretical, into electron–photon showers generated by cosmic rays. Particularly rapid progress was made in experimental studies owing to the use of the Wilson cloud chamber containing lead plates placed in a magnetic field. This made it possible to accurately determine the content and evaluate the spatial structure of the showers. In the opinion of one of the creators of shower theory, Heitler (p. 434 of Ref. 3), EPSs were first discovered for certain in the Wilson chamber.[4] The next important step forward in this

 1063-7796/94/020173-37$10.00

research was made when it became possible to obtain well collimated beams of gamma quanta.

The two approaches to the theory of electron–photon showers first appeared in 1937. These were the so-called successive-collision technique,[5] which, however, was not much developed further, and the analytic technique based on one-dimensional diffusion equations[6] in approximation A (i.e., neglecting ionization losses of shower particles) and in approximation B (i.e., assuming these losses to be constant). The solution of these equations, first obtained in approximation A,[7] is the cascade functions, i.e., the average numbers of electrons[2)] and photons in a given energy range and at a given depth in the absorber in which the shower generated either by a primary gamma quantum or by an electron is formed. Later the solutions of the diffusion equations were also obtained in approximation B. It should be emphasized that the solutions of the equations of one-dimensional cascade theory, including the approximate solutions were obtained for very severe simplifying constraints: complete screening, the absence of Coulomb scattering, asymptotic formulas for the bremsstrahlung emission and electron–positron pair production cross sections, and constant ionization losses. Therefore, they give a satisfactory description of the distribution of shower particles of very high energy in light media ($Z \lesssim 30$; Refs. 8–12). Approximation B was later introduced; in it the difference between the radiation bremsstrahlung and pair-production cross sections from the asymptotic cross sections was taken into account.[13] The applicability of approximation A of cascade theory was also extended to superhigh energies and very dense absorbers by including the LPM effect.[14]

However, owing to the angular dependence of the processes of bremsstrahlung emission, pair production, and, mainly, the multiple Coulomb scattering of shower electrons, which is particularly strongly manifested in absorbers consisting of heavy elements, the three-dimensional structure of real showers differs considerably from the one-dimensional structure. In other words, in a real shower developing in a sufficiently heavy medium, the electrons and photons are not transported along the direction of motion of the particle initiating the shower, i.e., along the shower axis, but instead they have a significant angular spread about this direction. This spread is the larger the lower the energy of the shower particles and the heavier the atoms of the medium. Therefore, the smearing of the EPS transverse to the shower axis is mainly due to the low-energy electrons and photons, and their numbers increase with the shower penetration depth. Nevertheless, this smearing is on the average small compared to the longitudinal dimensions of the shower, since low-energy electrons and photons are strongly absorbed in matter.

Estimates of the transverse shower dimensions in the form of the rms deviation angle of the shower particles and the rms distance from the shower axis can be obtained also using one-dimensional cascade theory, particularly for light absorbers.[11] However, a systematic description of the spatial structure of this phenomenon is possible only using a three-dimensional approach to the problem. The first attempts to create such a shower theory were made in 1940 (Refs. 15 and 16) and continued in later studies (Refs. 17–19; see also the reviews of Refs. 9 and 10 and the literature cited therein). Their main goal was the description of the electromagnetic component of extensive air showers in the case of heavy absorbers, which are of practical interest as detecting and shielding media, the diffusion equations of the three-dimensional cascade theory, which accurately take into account screening together with the energy dependence of the photon absorption coefficient and the scattering of shower particles, are so complicated that there are no analytic methods for solving them effectively,[10] and numerical solutions must be obtained by computer. Therefore, recently cascade theory has been successfully used in practice only to analyze experimental data pertaining to extensive air showers recorded by x-ray-emulsion chambers of various designs,[20] since the so-called axial approximation is valid in this case. Electron–photon showers developing in heavy absorbers and generated by particles of lower energy (tens of MeV and above) have been calculated using the Monte Carlo method of numerical modeling of the process, which is free of the constraints listed above.

In the first Monte Carlo study of showers generated in lead by electrons and photons of energy from 20 to 500 MeV, the numerical values corresponding to the phenomena taken into account were generated by a wheel of chance set in motion by an electric motor.[21] The motor in turn was initially turned off and on by hand by an operator, and then, in an improved version of the wheel of chance, it was turned off by a Geiger–Mueller counter activated by a cosmic ray several seconds after being turned on. Wilson calculated the cascade curves and compared them with the results of cascade theory and the experimental data. In the first case a clear discrepancy was obtained which indicated how important it was to include the multiple scattering of shower electrons. In the second case the agreement was satisfactory, which showed that the technique held promise.

In recent years a wide variety of programs have been written for the numerical modeling of electron–photon showers by computer. These programs take into account the elementary physical processes making up the EPS and the properties and configuration of the medium in which the shower develops with varying degrees of accuracy (see, for example, Refs. 22–24). Particularly noteworthy among them are programs of a universal nature, which are moreover constantly being improved by the inclusion of numerous suggestions made by users.[25–27] However, since the Monte Carlo method does not possess the common and often useful feature of clear physical interpretation and, moreover, it requires a great deal of computer time (this time usually grows linearly with energy[28]), it has become necessary to parametrize the main shower characteristics calculated by this method,[29,30] and also to develop new algorithms for fast modeling.[31–36] Banks (or libraries) of showers, both modeled numerically and measured experimentally, have been created for analogous reasons (for example, Refs. 37 and 38).

The Monte Carlo method is also used successfully at superhigh energies ($\sim$1000 TeV and above; Refs. 35, 39, and 40), which has made it possible to systematically take into account, in particular, the screening effect and the LPM effect. Here a hybrid approach, also known as the modified Monte Carlo method, is also used, in which the simulation is carried out until at each observation depth cascade particles are obtained with energy such that the average cascades from those particles are avaliable in previously established data banks.[40] Numerical modeling of EPSs by the Monte Carlo method has become particularly widespread in the prediction and optimization of the characteristics of various types of calorimeters (see, for example, Refs. 36 and 41–44), where the EGS-4 program[26] is commonly taken as the world standard. Moreover, this program is also used to estimate the effect of electromagnetic radiation on materials.[45]

There are quite a few works devoted to the experimental study of electron–photon showers. The overwhelming majority of them pertain to showers generated by electrons and only a relatively small fraction of them are concerned with showers initiated by photons. There are also studies in which showers were generated by positrons. The range of primary particle energies extends from 10 MeV to 200 GeV. Showers have been studied using various types of detectors: track devices—the Wilson chamber,[46–48] spark chambers,[49–53] photographic emulsions,[54] bubble chambers,[55–57] streamer chambers,[58] drift chambers (for improved spatial resolution),[59] counters [Čerenkov,[60–62] gas-discharge,[63] and scintillation[64,65]], position detectors [ionization chambers,[66] scintillation probes,[67] thermoluminescent dosimeters[68,69]], and also multilayer detectors composed of lead plates and sensitive materials [scintillators,[70–72] dosimeter glasses,[73] and stacks of x-ray film (Ref. 74)].[3)] The main goal of most of these studies has been to investigate the longitudinal and transverse development of showers in heavy amorphous media at energies of up to 10 GeV, in particular, the energy deposition profile, the energy dependence of the location of the maximum and the number of particles at the maximum, the energy dependence of the integrated shower path, and also fluctuations.

An important advantage of track detectors is the possibility of reconstructing the spatial structure of individual events, although, as a rule, the statistical accuracy is not high. On the other hand, position detectors can be sources of information only about the energy dissipation in an EPS. Experiments in which counters are used are considered the simplest. This method also ensures good statistical accuracy of the experimental results. However, in the simplest version only the averaged profile of the EPS can be determined in this way.[65]

The known methodological advantages of shower detectors compare favorably with those of electromagnetic calorimeters of various types and designs, particularly those constructed recently.[75,76] They have been used to measure the longitudinal and transverse profiles of the energy release in EPSs generated by electrons with energy from several GeV to 200 GeV (Refs. 77–88). In several studies carried out using these setups a deviation of the longitudinal shower profile from the exponential form at large absorber depths has been found (Refs. 77, 79, 81, and 83). The EPS radial distributions are most often approximated by the sum of two exponentials, one describing the relatively narrow hard core of the shower and the other describing its soft, diffuse component (Refs. 78, 82, 84, 87, and 88). However, the conditions which must be satisfied by calorimeters, namely, reliable particle identification and good energy and spatial resolution, require not only knowledge of the longitudinal and transverse shower profiles, but also of their fluctuations, the correlations of various EPS characteristics, and also the fluctuations of the position of the axis of a shower generated by a primary gamma quantum. A program to investigate all these characteristics of electron–photon showers produced by gamma quanta with energy in the range 100–3500 MeV has been carried out using the 180-liter xenon bubble chamber (XBC) at ITEP (Moscow).[89] A series of experimental studies using the technique of determining the gamma-quantum energy and studying the individual characteristics of EPSs initiated by gamma quanta were carried out earlier using the 24-liter XBC at JINR (Ref. 90).

The XBC offers unique possibilities for the detailed analysis of individual events of EPSs generated by gamma quanta with energy above $\sim$10 MeV. One of the main advantages of the XBC is the small value of the radiation length $t_0(\mathrm{Xe}) = (4.05 \pm 0.17)$ cm (Ref. 91)[4)] and the fairly clear depiction of tracks of electrons with energy greater than 0.5–1.5 MeV. In addition, the conversion point of the primary gamma quantum and the shower axis are accurately located, and the projected lengths of shower electron tracks can be measured on the average with a relative error of no more than 0.2. As an illustration, in Fig. 1 we show a typical electron–photon shower generated by a gamma quantum with energy of about 3 GeV recorded on a photograph at the 180-liter XBC at ITEP (Moscow). As a rule, it is also not difficult to separate the extraneous background coming from other charged particles, and to avoid errors related to the pileup of showers generated by two gamma quanta arising, in particular, in the decay of a high-energy π^0 meson. An example of an event of this type is shown in Fig. 2. The linear dimensions of these chambers are sufficiently large that, in addition to the advantages already listed, they are very useful detectors for studying EPSs in the energy range from several tens of MeV to several GeV. For example, the dimensions of the 24-liter XBC at JINR are $11\times7\times4.5$ r.l.,[90] and those of the 180-liter XBC at ITEP are $25\times11\times10$ r.l.[89]

In addition to the wide scope and diversity of problems solved, the results of EPS studies carried out using XBCs are of interest also because the shower characteristics of liquid xenon are close to those of many materials used as radiators in Čerenkov spectrometers. It should also be emphasized that detectors of hard electromagnetic radiation have recently been built in which liquid or even solid xenon is used as the active material, for example, the liquid-xenon calorimeter for recording EPSs from electrons and photons of energy from 1 to 10 GeV (Ref. 93). There has also been

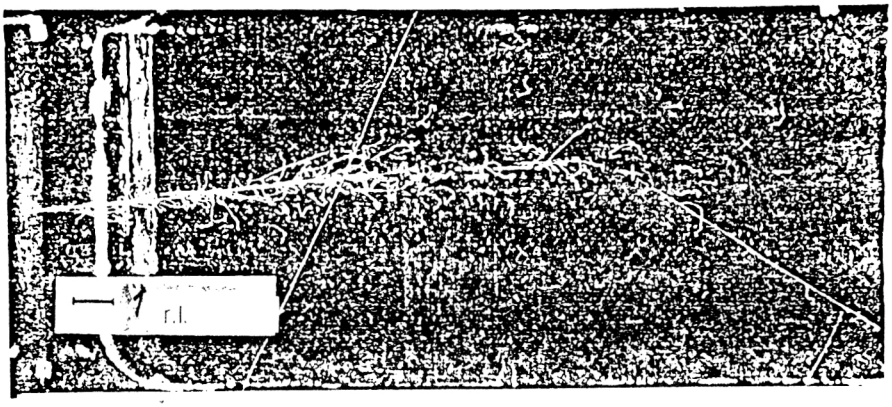

FIG. 1. An electron–photon shower induced by a gamma quantum of energy ~3 GeV, recorded in the 180-liter xenon bubble chamber at ITEP (Moscow). The radiation length is shown.

a proposition for a xenon detector consisting of a large number of cells (2×10^4) designed for colliding-beam accelerators of the next generation.[94] As is well known, detectors of this type must satisfy not only the criteria listed above, but also rather strict ones like uniform acceptance, linear response in a wide dynamical range, insensitivity to radiation damage for high loads of long duration ($>10^{33}$ cm$^{-3}\cdot$sec^{-1}), and short activation time. It turns out that most of these requirements are satisfied better by liquid xenon than by other scintillators (BGO, NaI(Tl), BaF_2, and TSM). In particular, it is practically insensitive to radiation damage (its radiation strength is greater than 10^7 rad; Ref. 94) and insensitive to magnetic fields; the degree of purity is not critical, and it offers the possibility of obtaining a ratio e/h close to unity.[95]

The goal of this review is to present the most important results pertaining mainly to the experimental study of electron–photon showers induced in dense amorphous media by gamma quanta and electrons of accelerator energies. Solid and detailed information on this topic is needed for solving a number of complicated problems of estimating the background and optimizing the characteristics of various types of presently existing and future electromagnetic and hadronic calorimeters, which, as already noted, must satisfy fairly strict requirements. In the next section we describe the main elementary physical phenomena making up an EPS and determine the parameters characterizing the spatial–dynamical picture of this process. The third section contains a brief review of the elements of cascade theory, with special emphasis given to those results which are of practical value at the present time. An alternative approach to the description of a cascade electromagnetic process based on modeling it numerically by the Monte Carlo method is briefly presented in Sec. 4. The results of experimental studies of various shower characteristics are reviewed in Sec. 5. There we also give a phenomenological scaling description of the longitudinal and transverse profiles of showers and their fluctuations obtained on the basis of analysis of the experimental results in the form of simple formulas convenient for practical use. This description often makes it possible to obtain sufficiently reliable quantitative estimates without resorting to awkward Monte Carlo calculations. The review is summarized in Sec. 6.

2. ELEMENTARY PROCESSES AND SHOWER PARAMETERS

The process of electron–photon shower formation can be represented as a succession of more elementary and independent interaction events undergone by each created shower particle. Although this is actually not a very rigorous representation (for example, Compton scattering on atomic electrons of the medium is accompanied by the ionization and excitation of these atoms), it is a useful simplification, the more so that it can be used to obtain a rather accurate description of the phenomenon in question. In addition, when studying the properties of showers it is common to use certain characteristic quantities depending only on the properties of the medium: the radiation length,[5)] the Molière unit, and the critical energy. It turns out that if the longitudinal and transverse dimensions of the EPS together with the primary and secondary energies

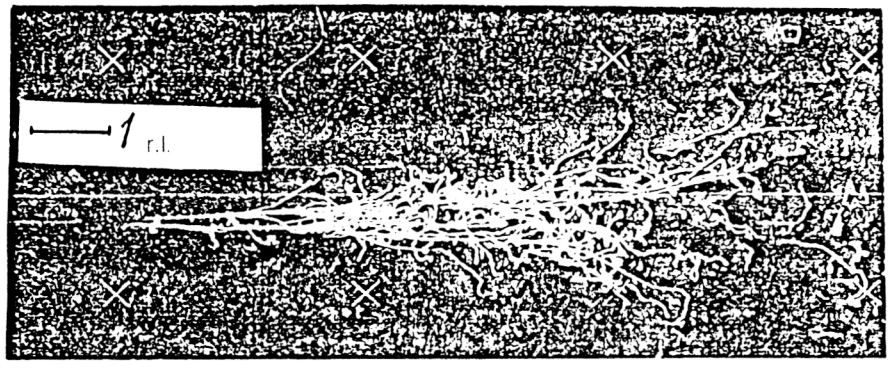

FIG. 2. Decay of a π^0 meson of energy ~3.5 GeV into two gamma quanta, which produce two closelying electron–photon showers. Photograph of the 180-liter XBC at ITEP (Moscow).

TABLE I. Notation and its description.

E_γ	gamma-quantum energy;
E'_γ	energy of secondary gamma quantum if the primary particle is a gamma quantum;
m	electron rest mass;
c	speed of light;
v	electron or positron speed; $\beta=v/c$, $\gamma=(1-\beta^2)^{-1/2}$;
E	total electron or positron energy in units of mc^2;
p	electron momentum in units of mc;
E'	total energy of the secondary electron or positron (in units of mc^2) if the primary particle is an electron or positron;
α	fine-structure constant;
r_e	classical electron radius;
e	electron electric charge;
h	Planck constant;
Z	nuclear electric charge (in units of e);
A	nuclear mass number;
t_0	radiation unit of length;
N_0	Avogadro's number;
ρ	density (g/cm^3);
I	atomic ionization potential;
$n=\rho N_0 Z/A$	concentration;
n	index of refraction.

are expressed in terms of these parameters, the dependence of the shower development on the medium in sufficiently heavy media is considerably weakened.

In this section we give the expressions for the probabilities of the main elementary processes making up the EPS, and we give the definitions of the shower parameters in question. We also give the limits of applicability of the formulas quoted. For convenience, the notation for physical quantities is given in Table I.

Electron–positron pair production by photons

The differential cross section for electron–positron pair production by a photon of energy E_γ in the field of an atomic nucleus integrated over angles can be written as[11,96]

$$\sigma_{ap}(E_\gamma,E)dE=4\alpha Z^2 r_e^2 \ln(183Z^{-2/3})(dE/E_\gamma)\psi(e_\gamma,E). \quad (1)$$

Since pair production occurs at some distance from the nucleus, the nuclear electric charge is screened by the atomic electrons. The effect of this screening is determined by the parameter

$$\xi\cong(136mc^2/E_\gamma)Z^{-1/3}/u(1-u), \quad (2)$$

which is proportional to the ratio of the effective atomic radius and the maximum value of the collision parameter. Here $u=E/E_\gamma$. The screening is assumed to be complete when $\xi\approx 0$, and absent if $\xi\gg 1$. We see from (2) that ξ decreases with increasing E_γ. Therefore, at high energies the primary gamma quanta are converted into electron–positron pairs with complete screening. Information on the screening in this process is contained in the function $\psi(E_\gamma,E)$. Graphs of it for air and lead at seven values of the energy E_γ are given in Figs. 3 and 4, respectively. The analytic approximation of this function commonly used at

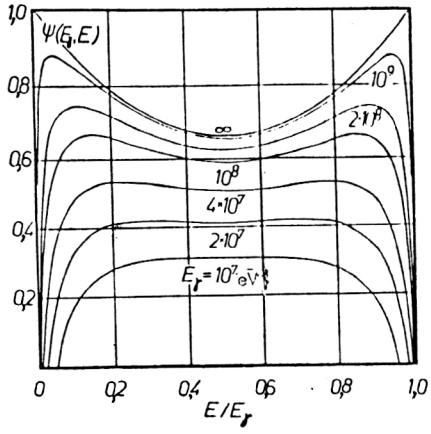

FIG. 3. Graph of the function $\psi(E_\gamma,E)$ describing the dependence of the effective cross section in air for the creation of an electron–positron pair by a photon of energy E_γ (Ref. 11). E is the energy of one of the particles of the pair.

present was obtained by Messel and Crawford[97] assuming the Thomas–Fermi potential with 1% accuracy.

At high energies electron–positron pairs are emitted in a very narrow angular cone in the direction of the primary photons. It is therefore usual to assume that the directions of motion of the pair and the gamma quanta created by it coincide. According to Ref. 97, as a criterion for the applicability of this approximation it is possible to use the ratio of the rms pair emission angle and the multiple scattering angle at a length of $t\approx 0.7$ r.l. In this case this ratio, which is approximately ln $E/30$, must be rather small.[97]

The total cross section for electron–positron pair production by a photon in the field of an atomic nucleus and atomic electrons has the form (Refs. 9, 11, and 98):

$$\sigma_p(E_\gamma,E)dE=4\alpha Z(Z+\xi)\ln(183Z^{-1/3}) \times r_e^2(dE/E_\gamma)\psi(E_\gamma,E), \quad (3)$$

where

$$\xi=\ln(1440Z^{-2/3})/\ln(183Z^{-1/3}) \quad (4)$$

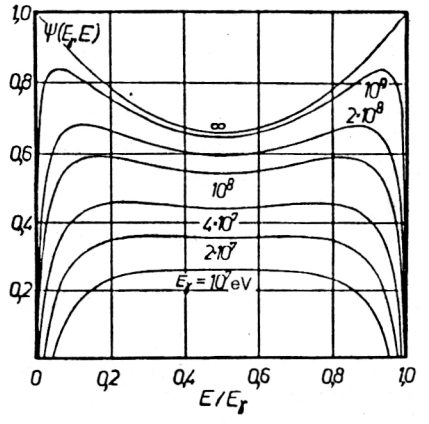

FIG. 4. The same as in Fig. 3 for lead (Ref. 11).

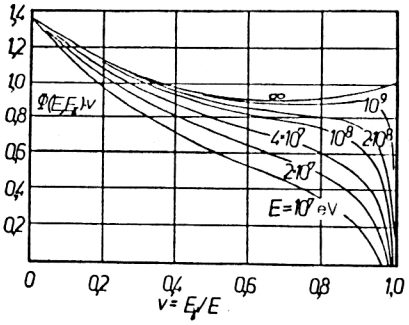

FIG. 5. Graph of the function $\phi(E,E_\gamma)$ describing the dependence of the effective cross section for bremsstrahlung with energy E_γ by an electron with energy E in air.

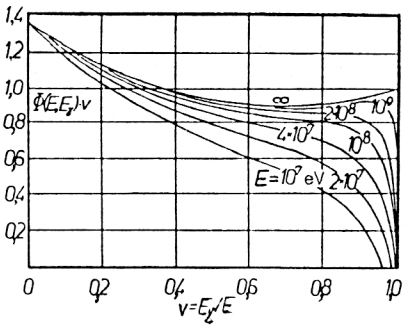

FIG. 6. The same as in Fig. 5 for lead (Ref. 11).

and varies from 1.33 at $Z=5$ to 1.16 at $Z=82$ (Ref. 96).

Since Eq. (3) was obtained in the Born approximation, which leads to values of σ_p which are too low at low energies, the semiempirical correction $A(Z)(\ln E_\gamma)/E_\gamma$ is added to the cross section (3) [for lead, $A(Z)=0.284$; Ref. 97]. In the case of superhigh energies, when the angle between the electron and the positron of the pair is very small ($\theta_p \approx mc^2/E_\gamma$), the longitudinal momentum transfer to the nucleus is small and, according to the uncertainty relation, the longitudinal dimensions $r_\parallel$ of the interaction region are increased considerably. In a sufficiently dense medium they can encompass many atoms, so that the rms angle of multiple scattering over a length $r_\parallel$ can turn out to be larger than the angle θ_p. Then, as shown by Landau and Pomeranchuk[99] and by Migdal,[100] in an amorphous medium the pair production probability is decreased compared to Eq. (3) (Ref. 97). For example, in lead this effect becomes important at $E_\gamma \gtrsim (2\times 10^{12}-10^{13})$ eV (Refs. 9 and 101).

Bremsstrahlung of the electron

The differential cross section for photon production by an electron in the field of a nucleus and atomic electrons integrated over angles has the form (Refs. 9, 11, and 98)

$$\sigma_b(E,E_\gamma)dE_\gamma = 4\alpha Z(Z+\xi)\ln(183Z^{-1/3}) \times r_e^2(dE_\gamma/E_\gamma)\phi(E,E_\gamma). \quad (5)$$

The screening effect is taken into account by the function $\phi(E,E_\gamma)$, as in the case of electron–positron pair production. An analytic approximation of this function has been obtained (with $\sim 1\%$ accuracy) using the Thomas–Fermi model of the atom.[97] Here the role of the screening parameter is played by the quantity

$$\xi \approx (136mc^2/E)Z^{-1/3}v/(1-v), \quad (6)$$

where $v=E_\gamma/E$. It is easy to see that at sufficiently high electron energies the electron radiation losses occur for practically complete screening. The dependence of the function $\phi(E,E_\gamma)$ on the energy E_γ of the emitted gamma quanta for several values of the energy E of the primary electrons in air and lead is shown in the Figs. 5 and 6, respectively. The angular spread of the secondary photons can be neglected, as before, if the quantity $\ln E/30$ is sufficiently small.[97]

For reasons analogous to those in the case of electron–positron pair production, the expression we have given for the effective cross section must be corrected. For example, at energies which are not very high the total cross section for bremsstrahlung (5) is multiplied by the factor $1+3(\alpha Z)^{1/3}/E$ a (Ref. 97). At ultrarelativistic energies ($E \gtrsim 10^{12}$ eV) the LPM effect leads to a decrease in the probability for the emission of lower-energy bremsstrahlung photons. For example, in lead the effective cross section for the production of photons with energy $E_\gamma < 10^{-3}E$ is smaller already at $E=10^{10}$ eV than expected when this effect is neglected. At higher electron energies the upper limit on the values of E_γ corresponding to a decrease of the cross section grows, and at $E=10^{13}$ eV it practically reaches a maximum, i.e., $E_\gamma \approx E$ (Refs. 9 and 10).

Excitation and ionization of atoms

Fast electrons and positrons undergo inelastic collisions with the atoms of the medium and lose their energy to excitation and ionization of these atoms. These are the so-called ionization energy losses. Expressions for the effective cross sections of electron and positron inelastic scattering on atomic electrons were first obtained by Moller[102] and Bhabha,[103] respectively. However, from the practical point of view it is convenient to use the macroscopic value of the average energy loss per unit of path traveled by the particle, which is known as the Bethe–Bloch formula.[104–111] For electrons it can be written as[112]

$$(-dE/dx)_{\text{ion}} = 2\pi r_e^2 mc^2\beta^{-2}n[\ln(mc^2EI^{-2}) + 0.43 + 2\ln(\beta\gamma) - \beta^2 - \delta]. \quad (7)$$

Here I denotes the average ionization potential of the atom and δ is a correction taking into account the effect of the density of the medium. The empirical approximation of the Z dependence of I in the range $Z \geqslant 13$ which is of greatest practical interest has been obtained by Sternheimer:[113]

$$I = 9.73Z + 58.8Z^{-0.19} \text{ eV}. \quad (8)$$

TABLE II. Contribution of the correction δ (in %) to the average ionization losees of electrons of energy E in various materials (Ref. 115).

E, MeV	H	O	Ne	A	C	Al	Cu	Pb
1	0	0	0	0	3.53	2.09	3.78	0.85
10	0	0	0	0	14.3	10.4	12.8	7.44
100	3.55	4.23	1.21	2.25	29.2	24.8	25.7	19.7

There are also other approximations of the Z dependence of the average (or effective) potential, for example, in the Thomas–Fermi model:[75,114] $I=16Z^{0.9}$ eV or simply $I=12Z$ eV. For complicated media the average potential is[115]

$$\ln I=\sum_i g_i \ln I_i,$$

where g_i denotes the ratio of the concentration of electrons in atoms of type i to the total electron concentration in the given material. The contribution of the correction δ depends on the particle energy and the properties of the medium. In Table II we give the results of calculations of the fraction which this correction contributes compared to the average ionization energy losses of electrons in various materials. It can be noted that as E increases the effect of the density of the medium grows. This increase compensates the logarithmic growth of the ionization energy losses, leading to the so-called Fermi plateau.[116]

It actually makes more sense to measure the decrease of the electron ionization energy losses due to the density of the medium relative to the total energy losses of electrons to collisions, ionization, and bremsstrahlung, which dominates at sufficiently high electron energies ($E\gtrsim 10$ MeV). Such estimates are given in Table III.

For complicated media the average electron ionization energy losses can be written as

$$\left(-\frac{1}{\rho}\frac{dE}{dx}\right)=\sum_i n_i\left(-\frac{1}{\rho}\frac{dE}{dx}\right)_i$$

where n_i is the concentration of the ith component of the medium.

The distribution of ionization energy losses of fast electrons in sufficiently thick layers of matter is asymmetric and characterized by a clearly expressed maximum arising from the large number of distant collisions, which lead to atomic excitation, and a long falloff, proportional to E^{-2}, arising from collisions at short distances and describing the energy distribution of electrons knocked out of atoms (so-called δ electrons). In other words, a fast electron in a medium undergoes on the average a large number of collisions in each of which it loses an insignificant fraction of its energy, and a small number of collisions in which it transfers a significant fraction of its energy, up to the maximum inclusive. The average energy losses $\bar{\Delta}=\overline{|x(dE/dx)|}$ in a layer of material of thickness x are related to the most probable values Δ_0 in this layer as[117]

$$(\bar{\Delta}-\Delta_0)\beta^2/(2\pi r_e^2 mc^2 N_0)=0.37x(Z/A).$$

A quantitative description of the fluctuations of the ionization energy losses was first obtained by Landay,[118] and then by other authors (Refs. 119–123; see also Ref. 75).

In those cases where high accuracy is not required, the average ionization energy losses of electrons and positrons with energy of at least 1 MeV can be approximated as[95]

$$-dE/dx=a-bE^{-c}\ [\text{MeV/cm}], \tag{9}$$

where the constants a, b, and c depending on the material are given in Table IV.

Coulomb multiple scattering

In a layer of matter of finite thickness a fast electron undergoes a number of quasielastic interactions with atoms, atomic electrons, and nuclei, as a result of which its energy can be decreased only insignificantly, but the direction of the particle motion is changed. In the simplest case, when the thickness of the layer is small and, therefore, the scattering angles θ are small, the probability density distribution $P(\theta)$ has the form[124]

$$P(\theta)d\theta=(2/\langle\theta^2\rangle)\exp|-\theta^2/\langle\theta^2\rangle|\,\theta d\theta, \tag{10}$$

where

$$\langle\theta^2\rangle=Z^2(N_0/A)(4cr_e^2/\alpha^2)\ln(181Z^{-1/3})/(E\beta^2)^2.$$

The problem of multiple Coulomb scattering in the general case has been solved by Molière[125] and other authors (Refs. 126–128 and 26). The numerical values of the functions which can be used to express the distribution in the scattering angle of electrons which have passed through a layer of matter of a given thickness are given in Ref. 97.

Compton scattering of gamma quanta

The differential cross section for the scattering of a gamma quantum on a free electron (Compton scattering) is described by the Klein–Nishina formula:[129]

TABLE III. The same as in Table II for the total energy losses of electrons in matter (Ref. 115).

E, MeV	H	O	Ne	A	C	Al	Cu	Pb
1	0	0	0	0	3,5	2,15	3,60	0,7
10	0	0	0	0	13,2	8,84	9,23	3,68
100	2,83	2,01	0,52	0,69	14,1	8,11	4,83	1,75

TABLE IV. Values of the constants a, b, and c in Eq. (9) (Ref. 97).

Material	a, MeV/cm	Electrons		Positrons	
		b	c	b	c
Pb	11,41	3,25	0,567	2,85	0,528
Al	3,84	0,59	0,768	0,45	0,704
C	11,31	2,32	0,574	1,92	0,516
Water	2,00	0,29	0,834	0,21	0,764
Emulsion (Ilford G5)	5,07	1,15	0,593	0,98	0,549

$$\sigma_c(E_\gamma, E'_\gamma)dE'_\gamma = \pi r_e^2 (mc^2 dE'_\gamma/E_\gamma)[1+u^2-2(1+k_0)/k_0^2 + (1+2k_0)u/k_0^2 + 1/(uk_0^2)]/u. \quad (11)$$

Here $u=E'_\gamma/E_\gamma$, $k_0=E_\gamma/mc^2$, and $1/(1+2k_0)<u<1$. It follows from energy and momentum conservation that the gamma-quantum scattering angle θ_γ and the recoil electron emission angle θ_e (relative to the direction of the primary photon) are given by the expressions

$$\cos\theta_\gamma = 1-(1/u-1)/k_0$$

and

$$\cos\theta_e = \sqrt{1-u}(1+1/k_0)/\sqrt{(1-u)+2k_0}.$$

The photoeffect

The photoeffect consists of the absorption of a photon by an atom with the subsequent emission of an electron possessing the energy of this photon decreased by the binding energy of the electron in the atom. The interaction occurs with electrons of the K shell if the photon has sufficiently high energy, or with electrons of higher shells if the photon energy is correspondingly lower. The cross section for this process obtained by Pratt[130] is approximated by the expression[97]

$$\sigma_{ph}(E_\gamma) = 4\pi r_e^2 mc^2 (\alpha Z)^4 (n/E_\gamma)\varphi(E_\gamma, Z), \quad (12)$$

where the αZ dependence of the coefficients of the expansion of the function $\varphi(E_\gamma, Z)$ in inverse powers of E_γ is given in numerical form in Ref. 97 (see also Ref. 117). The energy of the emitted electron is[97]

$$E = E_\gamma + [1-(\alpha Z)^2].$$

Electron–positron annihilation

The cross section for two-photon annihilation of an electron and positron was first obtained by Dirac (Ref. 3, p. 303):

$$\sigma_a(E) = \pi r_e^2 \frac{1}{E+1}\left[\frac{E^2+4E+1}{E^2-1}\ln(E+\sqrt{E^2-1}) - (E+3)/\sqrt{E^2-1}\right]. \quad (13)$$

For $E>2$ (i.e., positron energy above ~ 1 MeV) the cross section $\sigma_a(E)$ can be approximated by the simple expression[97]

$$\sigma_a(E) \approx 1.6\pi r_e^2 n E^{-7/9},$$

from which we clearly see that this process is important only at very low positron energies. The probability of one-photon annihilation of the positron on an atomic electron is less than 5% (Ref. 97).

Čerenkov radiation

A particle possessing electric charge Ze and moving with speed v greater than the speed of light in a given medium c/n, i.e., $v>c/n$, where n is the index of refraction of the medium, loses over a path of length dx an amount of energy dE in the form of electromagnetic waves at optical frequencies ν, with[131]

$$dE/dx = (2\pi Ze/c)^2 \int_{\beta n(\nu)>1} [1-1(\beta n)^2]\nu\, d\nu. \quad (14)$$

Since the number of photons emitted by the particle is proportional to $d\nu$ or, equivalently, $d\lambda/\lambda^2$ (λ is the wavelength of the emitted light), from (14) it follows that blue light dominates in Čerenkov radiation. If the dispersion of the medium, i.e., the λ dependence of n, is neglected, for optical wavelengths $\lambda=400$–700 nm from (14) we obtain

$$dE/dx = (Z\alpha/e)^2[(h\nu_1)^2-(h\nu_2)^2][1-1/(\beta n)^2]/2, \quad (15)$$

from which it follows that for a relativistic electron ($\beta\approx 1$) in water (n=1.33) $dE/dx \approx 400$ eV/cm, or 200 photons/cm, which makes up $\sim 0.02\%$ of its total energy losses.[132] It can also be noted that in the optical region the dependence of the Čerenkov radiation on the electron energy in a given material is determined by the factor $1-1/(\beta n)^2$. This dependence is shown in Fig. 7 for two materials: SF5 lead glass (n=1.67; Ref. 29) and liquid xenon (n=1.60; Ref. 95). We see from this figure that the electron energy losses to Čerenkov radiation simultaneously reach a plateau at an energy of 1–2 MeV, which is close to the frequently used value of the cutoff energy of shower electrons both in experiments (for example, Ref. 38) and in numerical modeling of showers (for example, Ref. 29).

Čerenkov radiation is characterized by a distinguished direction, which is determined by the angle θ relative to the

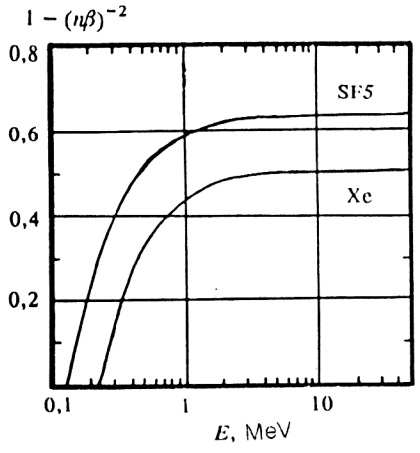

FIG. 7. Dependence on the electron energy of the factor $1-(n\beta)^{-2}$ determining the energy dependence of Čerenkov radiation in the optical region. The curves correspond to two materials: liquid xenon and SF5 lead glass.

velocity $v=\beta c$ of motion of the charged particle such that $\cos\theta=(c/n)/(\beta c)=1/(\beta n)$, $\beta>1/n$. Consequently, the front of the wave emitted by the particle moves, according to the Huygens principle, with speed $c/n<\beta c$ relative to the trajectory of this particle. Figuratively speaking, the electric field of a particle moving in a given medium having a smaller propagation velocity than the particle itself is continuously torn away from it until the condition $\beta>1/n$ is satisfied (see also Ref. 133).

It is appropriate to note that Allison, Cobb, and Wright[123,134] have obtained a unified description of the energy losses of a charged particle including ionization energy losses, Čerenkov radiation, and transition radiation, which arises as a result of the interference of Čerenkov radiation on the surface dividing two different media (see also Ref. 75, p. 8).

The Chudakov effect

A gamma quantum can be converted into an electron–positron pair such that in the laboratory frame (i.e., relative to the medium) the electron and positron each carry practically half the energy of the primary gamma quantum. If this energy is sufficiently large, the particles of the pair move so close to each other that their electromagnetic fields interfere. As a result, the bremsstrahlung and ionization energy losses of this pair are smaller than in the case of two similar but spatially separated particles, and so the range of the pair grows.[135] It is natural to expect that this effect influences primarily the initial stage of shower generation by a high-energy gamma quantum. In Fig. 8 we show an electron–photon shower generated by a cosmic gamma quantum with an energy of several hundred GeV, recorded in a photograph of the 180-liter XBC at ITEP (Moscow). Here the primary gamma quantum was probably converted in the chamber wall.[6)] From the point of entry of the electron–positron pair (A) to the start of intense shower production one can observe a barely noticeable straight track of length at least 3 r.l., the ionization density of which increases in going away from point A, but is significantly lower than that of electrons of another shower recorded alongside it.

In the simplest case, when the electron and positron of a pair have the same energy, the effective decrease of the ionization energy losses of the pair in the medium can be written as[124]

$$\Delta=(0.3072/\beta^2)\,[\beta^2/2+3\ln E-0.13-K_0(d/D)\,],$$

where $D=(4\pi r_e n)^{-1/2}$ is the screening radius, d is the distance between the electron and positron, and K_0 is the modified Bessel function of the second kind. In particular, the ratio of the pair energy losses to the sum of the energy losses of the electron and positron separately in nuclear emulsion is 0.46 over a path of length 15 μm and 0.86 over a path of length 200 μm if the pair energy is 180 GeV (Ref. 136).

Shower parameters

The structure of the effective cross sections of the two fundamental processes making up an EPS, i.e., the cross section for electron–positron pair production (3) and the bremsstrahlung cross section (5) are such that they can be represented as the product of two factors, one of which, pertaining not to a single atom but to the atomic concen-

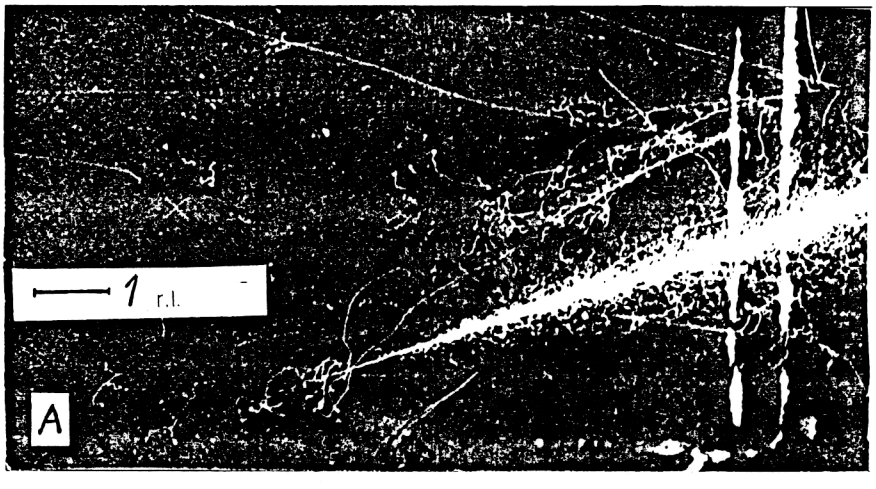

FIG. 8. An electron–photon shower induced by a cosmic-ray gamma quantum and recorded in the 180-liter xenon bubble chamber at ITEP (Moscow). Point A denotes the point of entry into the detecting volume of the chamber of the electron–positron pair into which the primary gamma quantum was converted. The radiation length is shown.

TABLE V. Numerical values of the radiation length t_0 and critical energy ε_c for several materials. Z is the (rms) atomic number and ρ is the density.

Material	Z	ρ, g/cm^3	t_0, cm	ε_c, MeV
Air	7.31	0.0012	30400	76
Water	4.69	1.00	35.7	62
Carbon	6	2.25	18.9	64
Aluminum	13	2.70	8.86	34
Nuclear Emulsion (Ilford G5)	21	3.83	2.88	14
Iron	26	7.86	1.74	18
Copper	29	8.94	1.42	16
Argon (liquid)	18	1.39	14.3	41.1*
Krypton (liquid)	36	2.45	4.76	21.3*
Xenon (liquid)	54	3.06	2.77	14.2*
BGO ($Bi_4Ge_3O_{12}$)	16.38	7.13	1.12	10.7
NaI	32	3.67	2.59	12.4
Lead	82	11.35	0.513	6.4

*Calculated using the data of Ref. 95 and Eq. (22).

tration n, contains information about the properties of the material in which the shower develops and has the dimensions of inverse length, while the second basically describes the dynamics of the process itself. For this reason it has proven useful to introduce the concept of the radiation length t_0, for which we give two of the rather many definitions. The first is of a general physical nature:[9,10]

$$1/t_0=4n\alpha Z(Z+\xi)r_e^2\{L_i^{\rm rad}-f(Z)\}[\text{cm}]. \tag{16}$$

Here $L_i^{\rm rad}=\int_0^{mc^2}|1-F(q)|^2dq/q+1$ and $F(q)$ is the atomic form factor. For heavy elements the Thomas–Fermi model of the atom gives $L_i^{\rm rad}=\ln(183Z^{-1/3})$, and $f(Z)$ is the correction for the Born approximation, $f(Z)\sim Z^2$ (Ref. 10). As before [Eqs. (4) and (5)], the quantity ξ includes the effect of the atomic electrons and is important at small Z, while the contribution from $f(Z)$ is important for heavy elements. The second expression for the radiation length is assumed to be generally applicable in practical calculations in the case of a homogeneous medium consisting of atoms of a single type with $Z\geqslant 5$ (Ref. 92, p. 51):

$$\begin{aligned}1/t_0=4\alpha r_e^2N_0(Z^2/A)[&\ln(184.15Z^{-1/3})\\&+\ln(1194Z^{-2/3})/Z-1.202(\alpha Z)^2\\&+1.0369(\alpha Z)^4-1.008(\alpha Z)^6/(1+\alpha^2Z^2)].\end{aligned} \tag{17}$$

The radiation length given by (16) has dimensions [cm], and in Eq. (17) its dimensions are [g/cm^2]. The conversion is done by multiplying or dividing by the matter density ρ [g/cm^3].

For matter consisting of several elements in the form of a mixture we have

$$1/t_0\approx\sum_i \omega_i/t_0^{(i)}, \tag{18}$$

where ω_i is the fraction (by mass) of the ith element with r.l. $t_0^{(i)}$. In the case of a chemical compound the value of t_0 is several percent smaller than obtained from (15) (Ref. 92, p. 51).

Using the concept of radiation length, we can express the average energy losses of the electron to bremsstrahlung in matter as

$$dE/dx=-E/t_0, \tag{19}$$

from which we find that the average energy of an electron which has travelled a distance x in the material is

$$E=E_0\exp(-x/t_0), \tag{19'}$$

where E_0 is the initial electron energy. The path x can be expressed in r.l., i.e., $t=x/t_0$. Then $E=E_0\exp(-t)$.

The second important shower characteristic, as noted in the Introduction, is the critical energy ε_c. It is defined from the condition that the amounts of energy lost to bremsstrahlung and to ionization be equal:[75]

$$\frac{(-dE/dx)_b}{(-dE/dx)_{\rm ion}}\cong\frac{Z\varepsilon_c}{580}=1, \tag{20}$$

from which we find $\varepsilon_c\cong 580$ MeV$/Z$.

The critical energy is also defined as the energy lost by the electron to ionization over a path of one r.l. (see Ref. 9, for example). Then instead of (19) we can write

$$dE/dt=-(E+\varepsilon_c). \tag{21}$$

Finally, the Molière unit is defined as (Ref. 75, p. 152)

$$R_M=21\ [\text{MeV}]\cdot t_0/\varepsilon_c, \tag{22}$$

or for $13\leqslant Z\leqslant 92$ with an error of less then 10% we can write[137]

$$R_M\cong 7A/Z. \tag{22'}$$

In Table V we give the numerical values of the radiation length and critical energy for several of the most commonly used materials.

In addition, for the liquid xenon with impurities filling the XBC (see the Introduction) $\rho=2.18$ g/cm^3, $t_0=(4.05\pm 0.17)$ cm (Ref. 91), and $\varepsilon_c=11$ MeV (Ref. 138). The values of t_0 and ε_c for many complex materials have been calculated in Ref. 139.

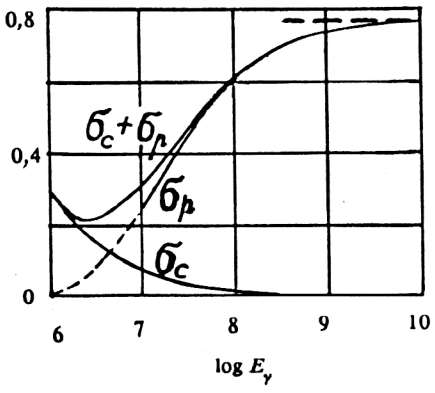

FIG. 9. Total cross sections per radiation length in lead for Compton scattering (σ_c) of photons of energy E_γ and for the production of an electron–positron pair by them (σ_p) (Ref. 11). The dependence of the sum of these cross sections on E_γ is also shown. The dashed line shows the asymptotic value of σ_p (E_γ is in eV).

Comparison of the cross sections

The relation between the cross sections for the fundamental processes making up an electron–photon shower in many respects determines its spatial structure. In Fig. 9 we show the dependence on the gamma-quantum energy E_γ of the total cross sections at 1 r.l. in lead: the Compton scattering cross section (σ_c), the electron–positron pair production cross section (σ_p), and the sum of these cross sections ($\sigma_c+\sigma_p$). It may be noted that the sum of the cross sections has a minimum at low energies E_γ ($E_\gamma\cong 4$ MeV in lead), so photons from this energy range will possess the highest penetrating power in the given material. It can therefore be expected that the longitudinal shower profile at large matter depths will mainly be determined by the law governing the absorption of just these photons, i.e., it will have a form $\sim\exp[-(\sigma_c+\sigma_p)_{\min}t]$, which has been established in a number of studies (for example, Ref. 97). Here t is expressed in r.l.

The average relative electron energy losses to ionization and bremsstrahlung in air and in lead are shown in Fig. 10. There the dashed line shows the asymptotic value of the radation energy losses, which in lead is reached at $E\cong 1$ GeV. The slight excess of this value above unity is due to the fact that at high energies, i.e., for complete screening, the average ionization energy losses to bremsstrahlung are[9] $(-1/E)(dE/dt)=1+b$, where $b=1/(18\ln(183Z^{-1/3}))$. For air $b=0.012$, and for lead $b=0.015$.

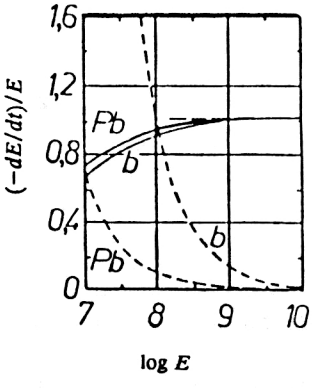

FIG. 10. Average relative energy losses of electrons to ionization (dashed lines) and bremsstrahlung (solid lines) in air (b) and in lead (Pb) (Ref. 11). The dashed line shows the asymptotic value of the radiation energy losses. The energy E is in eV.

3. MAIN RESULTS OF CASCADE THEORY

Several exhaustive review studies have now been published in which, as a rule, the foundations of the analytic approach to cascade theory have been discussed in great detail (Refs. 2 and 8–12). In addition, as already noted in the Introduction, the practical applicability of this approach is limited to very high energies of the particles initiating showers in fairly light materials ($Z\lesssim 20$–30). Nevertheless, some of the results concerning individual shower characteristics obtained by analytic methods are applicable also in the case of moderately high energies and heavier materials. This pertains mainly to integrated characteristics of EPSs, such as the energy dependence of the total track length of the shower electrons and the height and location of the shower maximum and its center of gravity. In this section we shall mainly give a brief discussion of precisely these results.

The equations and their solutions

The one-dimensional diffusion equations of shower electrons and photons taking into acount ionization energy losses, i.e., in approximation B, are written as[11]

$$\begin{aligned}\partial n_e(E_0,E,t)/\partial t=2&\int_E^\infty n_\gamma(E_0,E',t)\Sigma_p(E',E)dE'\\&+\int_E^\infty n_e(E_0,E',t)\Sigma_b(E',E'-E)dE'\\&-\int_0^E n_e(E_0,E_0,E',t)\Sigma_b(E,E')dE'\\&+\varepsilon\,\partial n_e(E_0,E,t)/\partial E;\end{aligned}\tag{23}$$

$$\begin{aligned}\partial n_\gamma(E_0,E,t)/\partial t=&\int_E^\infty n_e(E_0,E',t)\Sigma_b(E',E)dE'\\&-\int_0^E n_\gamma(E_0,E',t)\Sigma_p(E,E')dE'.\end{aligned}$$

In these equations Σ_p and Σ_b are the differential cross sections for electron–positron pair production (3) and bremsstrahlung (5), respectively, pertaining to a single r.l. of the material in which the shower develops; $n_e(E_0,E,t)$ and $n_\gamma(E_0,E,t)$ are the average numbers of electrons (n_e) and (n_γ) with energy in the range $(E,E+dE)$ at a depth t (in r.l.) along the development axis of a shower induced by a particle of energy E_0, and ε are the average ionization losses of shower electrons over 1 r.l. (i.e., the critical energy). If the shower is induced by a gamma quantum, then

$n_\gamma(E_0,E,0)=\delta(E-E_0)$ and $n_e(E_0,E,0)=0$, while if the primary particle is an electron, then $n_\gamma(E_0,E,0)=0$ and $n_e(E_0,E,0)=\delta(E-E_0)$.

It is the average numbers of particles of a given type with energy above some value E_c (the cutoff or threshold energy) that are actually of practical interest. These are the so-called cascade functions or cascade curves. In particular, for the electrons recorded by most detectors we have

$$N_e(E_0,E_c,t)=\int_{E_c}^{E_0} n_e(E_0,E,t)dE. \tag{24}$$

One of the most widely used and effective methods of solving Eqs. (23) is the method of moments.[2,10] It amounts to using these equations to find not the shower-particle distribution functions themselves, but to solving a simpler problem: that of determining their moments at depth t. Then, knowing all the moments, it is possible in principle to find the original functions. Here the zeroth moment or the so-called "equilibrium" spectrum (of electrons or photons) plays a basic role, since the recursion formulas can be used to successively calculate all the other moments of the particle distribution function.

The cascade functions of showers generated by gamma quanta in light materials are usually approximated by a Laguerre polynomial $L_n^1(x)$ with different weight functions, for example, $\gamma t\exp(-\gamma t)$. Then[10]

$$N_e(E_0,E_c,t)=\gamma t\exp(-\gamma t)\sum_{n=0}^{k} A_n L_n^1(\gamma t), \tag{25}$$

where A_n are the expansion coefficients and γ is a parameter taken equal to the absorption coefficient for low-energy photons, which have the greatest penetrating power (see Fig. 9, for example). In the case of primary electrons a sum of Laguerre polynomials can be used as the approximating function:[10]

$$N_e(E_0,0,t)=\left[\sum_{n=0}^{k} A_n L_n^0(\gamma t)+CL_{k+1}^0(\gamma t)\right]\times\exp(-\gamma t), \tag{26}$$

where the aditional term $CL_{k+1}^0(\gamma t)$ ensures satisfaction of the condition $N_e(E_0,0,0)=0$, and γ is as in (25). A weight function of the following form is used to construct the cascade functions of showers produced by gamma quanta in heavy materials:[10]

$$\omega(t)=\gamma^{i+1}t^i\exp(-\gamma t)/\Gamma(i+1), \tag{27}$$

where Γ is the gamma function, i is a parameter, and γ is as in (25). If the shower is produced by an electron, then[10]

$$\omega(t)=\gamma^{i+1}(a+t^i)\exp(-\gamma t)/[\Gamma(i+1)+a\gamma^i]. \tag{28}$$

The parameters i and a are determined from the condition of equality of the first moments of the desired particle distribution function and of the function $\omega(t)$ and the boundary condition $N_e(E_0,0,0)=1$.

The method of moments makes it possible to obtain the cascade functions and energy distributions at depths of $t\gtrsim 1$ r.l., at least in light materials, with $\sim 10\%$ accuracy. The series (25) and (26) converge sufficiently rapidly if the weight function is chosen appropriately. It has turned out, in particular, that the average distribution of the energy deposition along the shower axis or, equivalently, the longitudinal profile of showers induced by gamma quanta of energy above ~ 500 MeV in liquid xenon and by electrons at energies of several GeV producing showers in dense absorbers are satisfactorily parametrized by the function (27).

Moments of the cascade function

Of independent practical interest are the first moments of the cascade function and their dependence on the energy of the particle initiating the shower and on the properties of the medium in which the shower develops. From cascade theory in approximation B we find that the zeroth integrated moment or, in other words, the average value of the total range $\bar{R}=\bar{R}(E_0,E_c)$ of shower electrons with energy above E_c can be written in the following form (Ref. 2, p. 326):

$$\bar{R}=E_0[\exp(x)/\varepsilon_c][\varepsilon_1(x)-\varepsilon_1(x_0)\cdot x/x_0], \tag{29}$$

where $\varepsilon_1(x)=\int_1^\infty \exp(-sx)dx/s^2$, $x=qE_c/\varepsilon_c$, $x_0=qE_0/\varepsilon_c$, and $1/q=0.437$. In particular, if $E_c=0$, then from (29) we obtain

$$\bar{R}=E_0/\varepsilon_c. \tag{30}$$

The range–energy relation for shower electrons is of great practical value for determining the energy of gamma quanta recorded in track detectors with heavy material as the active medium, in particular, in the XBC, and also, owing to the independence of the Čerenkov radiation from the energy E of electrons with $E\gtrsim 1$ MeV (see Fig. 7), in total absorption Čerenkov calorimeters. The linear relation between the range and the electron energy in showers produced by gamma quanta in liquid xenon was first established by Z. Strugal'skiĭ[140,141] as a method of measuring the energy E_γ of gamma quanta in the XBC. Later studies led to a definitive expression for E_γ in terms of the average total range $\bar{R}$ of shower electrons:

$$E_\gamma=\alpha\bar{R}, \tag{31}$$

which is valid in the range $E_\gamma=20$–3500 MeV. Here $\alpha=(0.59\pm 0.02)$ MeV/mm (Refs. 142 and 143), and the electron cutoff energy is $E_c=0.5$–1.5 MeV. This result was then confirmed experimentally[144] and calculated by the Monte Carlo method.[145] The linear dependence between the integrated shower path and the primary electron energy in the range 150–550 MeV has also been obtained for lead[65] at the cutoff energy $E_c=5$ MeV.

The first integrated moment of the cascade function or, in other words, the center of gravity of the shower (or, equivalently, the average depth, or length, of the shower development) $\bar{t}$, together with the zeroth moment and the second moment, which is the longitudinal shower width, make it possible to estimate the height of the maximum of the cascade function, or, equivalently, the number of shower electrons at the maximum, if it is also assumed that near the maximum the cascade function is described by a

Gaussian distribution. In approximation B for showers generated by primary electrons with energy E_0 we have (Ref. 2, p. 338)

$$M_e^{\max}(E_0,0,t_{\max}) \approx 0.31(E_0/\varepsilon)/(\varepsilon\sqrt{\ln(E_0/\varepsilon)-0.1}). \quad (32)$$

Since the determination of the location of the shower maximum experimentally is not, as a rule, a difficult problem, especially at higher energies E_0 when the fluctuations of this location are relatively small, the energy E_0 can be estimated using the results of measurement of $N_e^{\max}$. In addition, the thickness of the material at which the maximum is located is considerably smaller than the thickness needed for total absorption of the shower energy, and the width of the maximum is relatively small ($\sim$1 r.l. at a primary gamma-quantum energy of $\sim$9 GeV; Ref. 146). Using considerations of this type, Tyapkin proposed a method of measuring the energy of gamma quanta and electrons with energy above 5 GeV and estimated that the energy resolution here is $\sim$10% (Ref. 147). It should also be noted that this method makes it possible to simultaneously estimate the energy of several gamma quanta or electrons emitted in a narrow solid angle, since there is no need for separate detectors with large transverse dimensions, as in the case of the total absorption method.[147] The suitability of using the relation between $N_e^{\max}$ and E_γ to determine the gamma-quantum energy in liquid xenon has also been indicated in Ref. 141, where it was noted that the accuracy of this method is 30% and 15% at energies of 1 and 5 GeV, respectively.

The relation between $N_e^{\max}$ and the energy of the gamma quanta initiating the shower has been determined experimentally for liquid xenon in the range E_γ=1600–3400 MeV (Ref. 148):

$$N_e^{\max} = (4.0\pm0.7) + (2.9\pm0.3)E_\gamma .$$

Here E_γ is in GeV and the shower electron cutoff energy is $E_c = (3.5\pm1.2)$ MeV. The energy resolution is $\sim$20% and is practically constant over the entire range of E_γ. The following approximation has been obtained for showers produced in lead by electrons of energy E=2–15 GeV (Ref. 72):

$$N_e^{\max} = 10.71E^{0.935},$$

and the shower electron cutoff energy is E_c=7.4 MeV.

The dependence of the center of gravity $\bar{t}$ of the shower electron distribution on the energy E_0 of the particle producing the shower can be written as follows, in approximation B, for primary electrons:[2,11]

$$\bar{t}(E_0,0) = 1.01\ln(E_0/\varepsilon) + 0.4, \quad (33)$$

and for primary photons:[11]

$$\bar{t}(E_\gamma,0) = 1.01\ln(E_\gamma/\varepsilon) + 1.2. \quad (34)$$

The experimentally measured dependence of $\bar{t}$ on E_γ for liquid xenon in the range E_γ=100–3500 MeV has the form[149]

$$\bar{t}(E_\gamma) = a_t + b_t \ln E_\gamma , \quad (35)$$

where $a_t = -4.84\pm0.09$ r.l., $b_t = 1.32\pm0.03$, and E_c=0.5–1.5 MeV. It turns out that the longitudinal distribution of ionization energy losses in the shower expressed in units of $\bar{t}(E_\gamma,E_c)$ is practically independent of E_γ in the range $E_\gamma \approx$ 500–3500 MeV. The only exception is the small interval $x = t/\bar{t}(E_\gamma) \lesssim 0.15$ at the start of the shower, where the dependence of multiple Coulomb scattering on the energy of the electrons and positrons arising as a result of conversion of the primary gamma quanta is important.

The linear relation between $\bar{t}(E_\gamma)$ and $\ln E_\gamma$ also follows from the results of numerical modeling of EPSs by the Monte Carlo method for SF5 lead glass in the energy range E_γ=100–5000 MeV (Ref. 29). Measurements performed using an Si/W sandwich calorimeter show that it also occurs for showers induced by electrons of energy E=4–49 GeV (Ref. 81):

$$\bar{t}(E) = (8.4\pm0.5) + (0.45\pm0.17)\ln E,$$

where E is in MeV and $\bar{t}$ is in r.l.

The maximum of the cascade function in approximation B for showers generated by gamma quanta is (Ref. 2, p. 308)

$$t_{\max}(E_\gamma,0) = 1.01[\ln(E_\gamma/\varepsilon) - 0.5], \quad (36)$$

and differs only insignificantly from the analogous quantity obtained by the Monte Carlo method for the range E_γ=100–5000 MeV and E_c=0.5 MeV in lead glass:[29]

$$t_{\max}(E_\gamma,0.5) = 1.16[\ln(E_\gamma/\varepsilon) - 0.62].$$

The dependence of $t_{\max}$ on the primary electron energy E in the range 4–49 GeV determined experimentally for tungsten has the form[81]

$$t_{\max}(E) = (3.97\pm0.24) + (1.02\pm0.11)\ln E.$$

An analogous approximating function has been obtained for showers generated by electrons with energy from 2 to 15 GeV in lead:[72]

$$t_{\max}(E) = 3.9 + \ln E,$$

E_c=7.4 MeV. For convenience, in Table VI we give these shower characteristics in approximation B.

Fluctuations

An important and complex problem of direct practical interest for studying and detecting EPSs is that of fluctuations in the fraction of energy absorbed in a fairly thick layer of material. Uchaĭkin and Lagutkin have derived equations for the distribution function of the absorbed energy, and also for the first and second moments of this distribution, and have determined the asymptotic relations between the relative fluctuations of the absorbed energy $\delta Q_{e,\gamma}$ and the particle number fluctuations $\delta N_{e,\gamma}$ in approximation B of cascade theory:[150]

$$\delta Q_{e,\gamma} = (\varepsilon/|\lambda_1(s)|)(\bar{N}_{e,\gamma}/\bar{Q}_{e,\gamma}).$$

Here $\lambda_1(s)$ is a parameter determining the form of the cascade function at various shower development depths (Ref. 11, p. 275), $\bar{N}_{e,\gamma}$ is the average value of the number

TABLE VI. Shower characteristics in approximation B (Ref. 2, p. 308): $x=E/\varepsilon$, $\bar{R}$ and t are in r.l., and $E_c=0$.

Quantity	Primary photon	Primary electron
Total mean free path of shower electrons, $\bar{R}$	x	x
Average shower depth, $\bar{t}$	$1.01\ln x+1.2$	$1.01\ln x+0.4$
Location of shower maximum, $t_{\max}$	$1.01(\ln x-0.5)$	$1.01(\ln x-1)$
Height of shower maximum, $N_e^{\max}$	$0.31x/\sqrt{\ln x-0.18}$	$0.31x/\sqrt{\ln x-0.37}$

of shower electrons in a given layer of material, and $\bar{Q}_{e,\gamma}$ is the average value of the energy absorbed in this layer. The subscripts e and γ refer to these quantities for showers generated either by electrons or photons; $\delta Q_{e,\gamma}=\sqrt{\bar{Q}^2_{e,\gamma}-\bar{Q}^2_{e,\gamma}}/\bar{Q}_{e,\gamma}$ and $\delta N_{e,\gamma}=\sqrt{\bar{N}^2_{e,\gamma}-\bar{N}^2_{e,\gamma}}/\bar{N}_{e,\gamma}$.

The question of fluctuations, i.e., the probability distribution $W(N_e)$ of the number N_e of shower electrons, has not been satisfactorily resolved in cascade theory. If the shower electrons were genetically independent, then $W(N_e)$ would be a Poisson distribution with a single parameter, namely, the average value $N_e(E_0,E_c,t)$ determined by Eqs. (24) and (23). However, this assumption is approximately valid only near the shower maximum (see Ref. 56, for example). It turns out that the Pólya distribution is a satisfactory approximation of $W(N_e)$ over the entire shower depth beginning at $t=1$ r.l. This conclusion follows from comparison of the results of numerical modeling of the EPS and the attendant fluctuations using this distribution. The modeling was done for lead glass in the primary photon energy range $E_\gamma=100$–5000 MeV (Ref. 29). Finally, we note that the method of random moments is also used to study the fluctuations in high-energy electron–photon showers.[151]

4. NUMERICAL MODELING OF ELECTRON–PHOTON SHOWERS

The most universal approach to the description of electron–photon showers is at present the Monte Carlo numerical modeling of the process. This approach makes it possible to take into account the wide variety and specific features of the physical phenomena making up an EPS, along with the external conditions (for example, a magnetic field), the spatial structure (which, as a rule, is complicated), and the properties of the medium (which is often inhomogeneous) in which the shower develops. The approach based on Monte Carlo (MC) modeling of an EPS is essentially free from any fundamental limitations. It makes it possible to obtain a specific result in numerical form, so it is frequently used in such practically important problems as the determination of the detection efficiency, the spatial resolution, and also the study of the diverse background effects arising in existing and future electromagnetic calorimeters. In addition, the MC method can be used successfully to calculate radiation shielding and to estimate the radiation and thermal effects induced by hard electromagnetic radiation in various materials. The MC method can also be used to study various characteristics of EPSs and their dependence on the primary particle energy. For this one essentially performs a numerical experiment, i.e., one uses existing computer programs [for example, EGS (Ref. 26) or GEANT (Ref. 27)] to generate some optimal set of showers (usually several hundred to several thousand showers; Refs. 29 and 30) induced in a specific material by particles of a given type with energy in some range. From this one then obtains the distributions of interest (primarily the longitudinal and transverse profiles) and parametrizes them by functions selected from general physical considerations. This approach is also applicable in the experimental study of EPSs, where it is referred to as phenomenological modeling.[152]

Fundamentals of the method

The numerical modeling of an EPS is in principle no different from similar problems in which the Monte Carlo method or, equivalently, the method of statistical sampling, is used (see Ref. 153, for example). The main features are the construction of an adequate probabilistic model of the phenomenon, including elementary interactions and radiation transport (i.e., particle motion), and also organizing the calculation and data storage.

In the modeling process the fate of each shower particle is followed as long as the particle is located inside a given volume of material and its energy exceeds some fixed value: the cutoff energy. The computation is carried out such that at the very top of the computer memory is stored the data pertaining to the particle with the lowest energy, and the fate of this particle is followed. If new particles appear as the result of an interaction, they are placed in the memory at levels determined by their energies. Here the volume of memory is kept within $\log_2(E_0/E_c)$, where E_0 is the energy of the primary particle generating the shower. The computation stops when all the shower particles are extracted from the memory. The needed information is stored throughout the computation.

The characteristics (energies, emission angles, mean free paths) of shower particles are simulated in accordance with the appropriate effective cross sections (see Sec. 2) represented as probability distributions using a random-number (more precisely, quasi-random-number) generator. For example, the random quantity x can be obtained from the distribution with probability density $f(x)$ by solving the equation

$$r=\int_0^{x(r)} f(t)dt \tag{37}$$

for $x(r)$, where r is a random number from a set uniformly

TABLE VII. Values of the parameters A, α, and b in Eq. (40).

E_γ, MeV	N	A	α	b	$\bar{t}$	t_{max}
100	1500	4,54	1,00	0,515	3,88	1,94
300	1500	7,18	1,45	0,493	4,97	2,94
500	1900	8,24	1,65	0,476	5,57	3,47
700	1300	8,32	1,84	0,470	6,04	3,91
1000	1700	8,58	2,03	0,468	6,47	4,34
5000	650	10,88	2,74	0,454	8,24	6,04

The lengths $\bar{t}$, t_{max}, and $1/b$ are expressed in r.l. The data are from Ref. 29.

distributed in the range 0–1 (Refs. 154 and 155). In particular, if it is necessary to determine the mean free path of a particle to the next interaction event, then

$$f(x)=\exp(-x/\lambda)/\lambda, \tag{38}$$

and, according to (37), $x=-\lambda \ln r$. Here λ is the mean free path of this particle $\lambda=1/n\sigma_t$, n is the concentration of atoms of the medium, and σ_t is the total cross section for interaction with an atom (molecule) of the medium. In general, $\lambda=\lambda(x)$, and, using the concept of accumulated probability $F(x)=\int_0^x f(t)dt$, we can write down an expression for the probability that the particle interacts on the path segment from x_0 to x:

$$F(x)=1-\exp[-\bar{n}(x)],$$

where $\bar{n}(x)=\int_{x_0}^x dt/\lambda(t)$ denotes the number of mean free paths travelled by the particle on this segment. However, for most functions of interest from the viewpoint of EPS modeling it is difficult to solve Eq. (37), and an algorithm which is a generalization of the discarding technique (Ref. 156; see also Refs. 26 and 97) has become widely used. It amounts to the following. If a function $f(x)$ can be written as

$$f(x)=\sum_{i=1}^{n} \alpha_i f_i(x) g_i(x), \tag{39}$$

where $\alpha_i>0$, $i=1,2,...,n$; $0\leqslant g_i(x)\leqslant 1$, $f_i(x)\geqslant 0$ for all x from the region of definition of $f_i(x)$ and $\int f_i(x)dx=1$ in this region, then the random variable x can be determined by the following procedure:

1. Choose from the uniform distribution a number i $(1\leqslant i\leqslant n)$ with probability proportional to α_i.

2. Choose a variable x from the distribution $f_i(x)$ [for example, using Eq. (37)].

3. Calculate $g_i(x)$ and choose a random quantity x' from the uniform distribution in the interval from 0 to 1. If $g_i(x)>x'$, the random quantity x is taken. Otherwise, the entire procedure is repeated from the beginning.

The probability of a suitable choice is $1/\Sigma_{i=1}^n \alpha_i$ and the average number of attempts is $\Sigma_{i=1}^n . \alpha_i$ As an example, let us take the normal distribution $f(x)=2/\pi \exp \times(-x^2/2)$ $x\geqslant 0$. Then the expansion (39) takes the following form.[97] (1) For $0\leqslant x<1$: $\alpha_1=\sqrt{2/\pi}$, $f_1(x)=1$, $g_1(x)=\exp(-x^2/2)$; (2) for $x\geqslant 1$: $\alpha_2=1/\sqrt{2/\pi}$, $f_2(x)=2\exp[-2(x-1)]$, $g_2(x)=\exp[-(x-2)^2/2)]$. The average number of attempts is $\alpha_1+\alpha_2\cong 1.2$.

Although, as already noted, at present there are universal and commonly used programs for modeling EPSs, problems can sometimes arise in which it is appropriate or even necessary to obtain certain information, in particular, of a methodological nature, and for this the MC method is practically the only one which can be used.[157,158]

Fundamental results

Among the numerous results obtained by the MC method it is particularly appropriate to mention the parametrization of the longitudinal and transverse profiles, and also the study of the fluctuations in EPSs induced by gamma quanta of energy from 100 MeV to 10 GeV in lead glass.[29,30] These results have more general value and make it possible to predict the development of showers in a dense uniform medium, which is of practical interest, and to estimate a number of important quantities of a methodological nature without resorting to complicated calculations. In addition, they are often used for comparison with the corresponding experimental data.

After modeling a total of 8550 showers induced by gamma quanta with energy E_γ in the range 100–5000 MeV in lead glass (1 r.l.=2.36 cm), Longo and Sestili[29] described the distribution of the average number $N_e(E_\gamma, E_c, t)$ of shower electrons with energy above $E_c=1$ MeV (the total energy) by a function analogous to the weight function (27):

$$N_e(E_\gamma, E_c, t)=At^\alpha \exp(-bt). \tag{40}$$

The modeling was carried out to a shower development depth of 15 r.l. The values of the parameters A, α, and b, and also the number N of modeled showers at a given energy E_γ are given in Table VII. There we also give the values of the center of gravity $\bar{t}$ calculated using the data of Ref. 29 and the locations t_{max} of the shower maximum.

The cascade function (40) can be related to the total mean free path $\bar{T}_i(E_\gamma)$ of shower electrons observed in a layer of material of thickness Δt ($\Delta t=0.5$ r.l.) at a depth $t=(i-1)\Delta t$ $(i=1,2,...,50)$ (Ref. 29):

TABLE VIII. Average man free paths $\bar{R}$ of shower electrons in lead glass of thickness $L=5$, 10, and 15 r.l. and the rms deviations ΔR corresponding to them (Ref. 29).

E_γ, MeV	$L=5$		$L=10$		$L=15$	
	$\bar{R}$, cm	ΔR, cm	$\bar{R}$, cm	ΔR, cm	$\bar{R}$, cm	ΔR, cm
100	12,7	4,6	16,7	1,8	17,3	0,8
300	31,3	12,2	48,1	6,4	51,9	2,0
500	45,2	20,0	78,3	10,6	86,1	3,6
700	56,1	26,6	106,6	15,8	120,0	5,2
1000	71,8	35,3	147,3	23,9	168,9	8,4
5000	210,0	127,0	647,0	152,0	843,0	75,0

$$\bar{T}_i(E_\gamma)=\int_{(i-1)\Delta t}^{i\Delta t} N_e(E_\gamma,E_c,t)dt. \tag{41}$$

It should be noted that analogous modeling[30] performed using the program GEANT 3.11 (Ref. 27) for identical conditions (the same SF5 lead glass and the same development depth and cutoff energy) leads to rather different results for α and $1/b$ (differing by 10–15%) at the same values of E_γ, while the energy dependence of the normalization factor A is completely different. Nevertheless, this has practically no effect on the location of the maximum $t_{\max}$ and the value of the center of gravity $\bar{t}$ in the range of energies E_γ considered; the difference is less than 2–4%, but it increases systematically with increasing E_γ.

The radial distribution of the energy release summed over the shower depth was approximated satisfactorily by the function[30]

$$f_r(r)=C\exp(-r/\mu), \tag{42}$$

where r is the distance from the shower axis and μ is a parameter (the so-called attenuation length). The modeling was performed for 6 values of the gamma-quantum energy: 200 (12 500), 500 (5000), 1000 (2500), 2000 (1250), 5000 (500), 10 000 (150) MeV, where the number of modeled events is given in parentheses. The dependence of the parameter μ on the shower development depth t was approximated by the function[30]

$$\mu(t)=B\exp(t/t_s)^{1/2}, \tag{43}$$

where $t_s=0.16[\log E_\gamma-1]$, with $B=0.039$ and E_γ in MeV.

Therefore, the three-dimensional distribution of the mean free path (or the energy deposition) in showers generated by gamma quanta with energy $E_\gamma=200$–– 10 000 MeV in lead glass can be expressed, according to Ref. 30, as

$$F(r,t)=t^\alpha\exp(-bt)\cdot g(t,r), \tag{44}$$

where the radial distribution normalized to unity is

$$g(t,r)=\exp[-r/\mu(t)]/\mu(t).$$

The longitudinal fluctuations of the electron mean free paths in showers generated by gamma quanta of energy $E_\gamma=100$–5000 MeV in lead glass have also been modeled.[29] In Table VIII we give for six values of the energy E_γ the mean free paths of electrons in lead glass of thickness 5, 10, and 15 r.l. and their corresponding rms deviations.

We see from these data, in particular, that owing to the significant longitudinal fluctuations the measurement of the gamma-quantum energy in a Čerenkov counter of insufficient thickness leads not only to large statistical errors, but also to large systematic ones. We also recall (see Sec. 3) that the numbers $n=N_e(E_\gamma,E_c,t)$ of shower electrons at a depth t (for $t\geqslant 1$ r.l.) are satisfactorily described by the Pólya distribution:[29]

$$P_i(n)=[\lambda_i/(1+b_i\lambda_i)]^n\{1[1+b_i]\ldots \times[1+(n-1)b_i]/n!\}P_i(0), \tag{45}$$

where $P_i(0)=(1+b_i\lambda_i)^{-1/b_i}$. The modeling was done with a depth step of $\Delta t=1$ r.l. for lead glass with infinite transverse dimensions for nine values of t ($i=1,2,\ldots,9$). Here the exponential distribution of the conversion lengths of the primary gamma quantum initiating the shower was taken into account. The values of E_γ for which the modeling was performed are given in Table VII. The numbers λ_i and b_i were taken to be free parameters of the distributions and were calculated according to the χ^2 criterion from comparison of the n distributions modeled by the MC method with the function (45). They are related to the average value $\bar{n}_i$ of the number of particles at depth $t=i$ r.l. and its dispersion σ_i^2 as

$$\lambda_i=\bar{n}_i,\quad \sigma_i^2=\bar{n}_i(1+b_i\bar{n}_i).$$

5. EXPERIMENTAL STUDY OF SHOWERS

The subject of study in most of the experimental research devoted to electron–photon showers has been the development of this process along the direction of motion of the particle initiating the shower. The average longitudinal profiles of the EPS have been measured primarily in the form of the distribution of the number of shower electrons (see, for example, Refs. 51, 56, 57, 65, 71, 85, and 159–161), the mean free paths (Refs. 152, 158, and 162–165), and the energy deposition by detection of the light effect (luminescence,[69,73] Čerenkov radiation,[60–62] and ionization energy losses (Refs. 74, 79, and 83). Experimental studies on the transverse development of EPSs have begun to appear only relatively recently and are mainly related to the solution of methodological problems pertaining to the

optimization, calibration, and installation of electromagnetic calorimeters of various types (Refs. 59, 69, 82–84, and 86–88), although the first studies on this topic were published considerably earlier (Refs. 159, 160, 73, 152, 165, and 166). There are a few studies in which more subtle but very important shower features were investigated, namely, fluctuations (Refs. 56, 57, 149, 152, 159–161, 165, and 167–170) and correlations between various EPS characteristics (Refs. 149, 169, and 171). Practically all the studies in this last area were performed using xenon bubble chambers.

In this section we present the main results (aside from those of Sec. 3 above) of experimental studies of showers induced in heavy amorphous media by gamma quanta and electrons with energy from 100 MeV to 200 GeV. Since, as already noted, a significant contribution to this research has been made using xenon bubble chambers (in particular, the 180-liter XBC at ITEP) and the results of those studies will be discussed below, we shall first briefly dwell on the most important methodological questions related to study of EPSs using XBCs.

Study of showers using XBCs

The energy of the gamma quanta inducing showers in XBCs is determined by Eq. (31) (Ref. 141). In the scanning of XBC photographs EPS events are selected which satisfy the following criteria: (1) the shower axis lies in the plane of the photograph, (2) there are no background tracks in the photograph which would complicate the analysis of the recorded event. The average magnification of a photograph is 0.94 (here and below we refer to Refs. 38, 149, 158, 162, and 166–173). In the selected EPS events a curvometer was used to measure, in the plane of the photograph, the total mean free path $\bar{R}$, the potential length L_{pot} of the shower development, i.e., the distance, along the shower axis, from the primary gamma-quantum conversion point to the point of intersection with the chamber wall, and the maximum length t_m of the shower development, measured from the start of the shower (i.e., the primary gamma-quantum conversion point) to the end of the last observed shower electron track along the EPS axis. Then the t_m distributions of L_{pot} were constructed for the ranges of energy E_γ for the showers selected in the scanning. An example of such a scatter plot for three energy ranges is given in Fig. 11. For further analysis we took only those events whose potential development lengths were at least $L_{\min}(E_\gamma)$, equal to the maximum t_m in a given range of energy E_γ. (In Fig. 11 these values are indicated by arrows for the corresponding ranges of E_γ.) This is the third selection criterion. The goal of this procedure is to decrease the effect of cutoff of showers recorded by a detector of finite thickness, and also to eliminate the possibility of preferential selection of showers with smaller values of t_m (i.e., apparatus "shortening" of the showers). For each shower satisfying these three selection criteria measurements were made (in the plane of the photograph) of the summed paths of the shower electrons $\Delta\Sigma r(t,p|E_\gamma)/\Delta t\Delta p$ observed in rectangular cells of the grid with sides $\Delta t=0.6$ r.l. along the shower axis and Δp

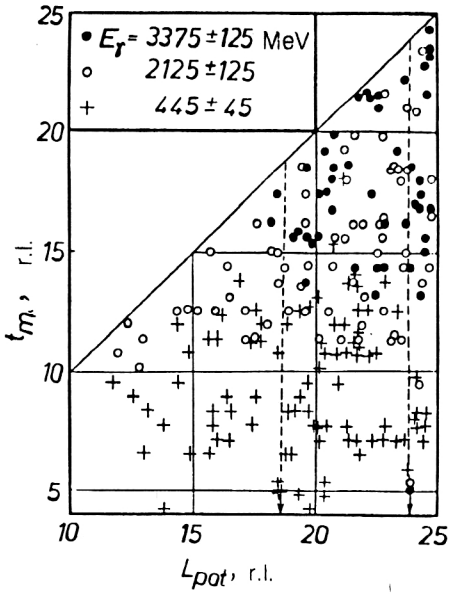

FIG. 11. Scatter plot of showers generated in liquid xenon by gamma quanta of energy E_γ; L_{pot} is the potential development length and t_m is the maximum development length. The arrows indicate the values of the minimal L_{pot} for a given E_γ (according to the selection criteria; Ref. 38).

$=0.3$ r.l. in the perpendicular direction. The minimum path length is ~ 2 mm, which corresponds to an electron energy of ~ 0.5 MeV (Ref. 115). Figure 12 illustrates a typical example of a shower in the plane of the photograph and the grid on which the summed paths $\Delta\Sigma r(t,p|E_\gamma)/\Delta t\Delta p$ were measured. The origin of the grid ($t=p=0$) coincides with the primary gamma-quantum conversion point, and the t axis is directed along the

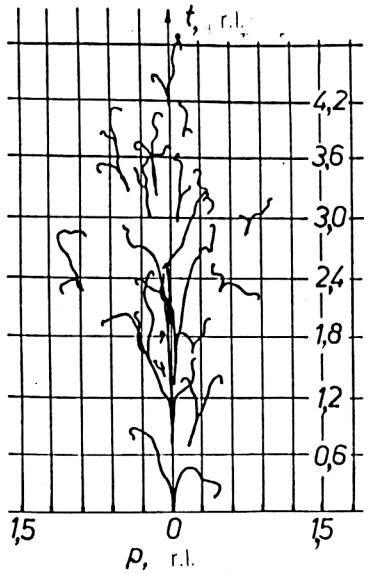

FIG. 12. Schematic depiction of a shower recorded on a photograph of the XBC and the grid used to measure the summed paths of shower electrons.

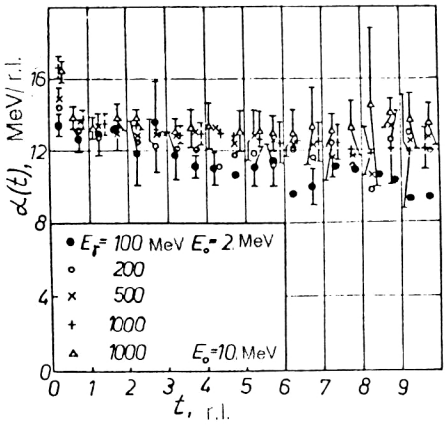

FIG. 13. Distribution of $\alpha_p(t)$, defined by Eq. (47), in the development length t of showers produced by gamma quanta of energy E_γ in liquid xenon. E_0 is the photon cutoff energy used in the modeling.

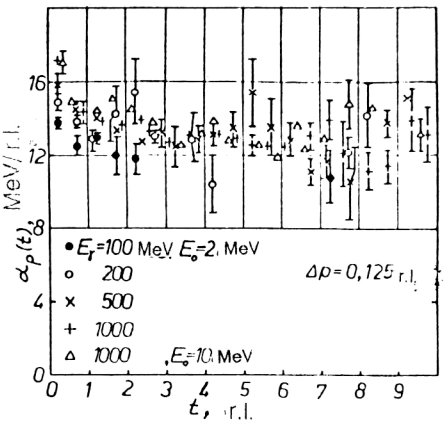

FIG. 14. The same as in Fig. 13 for $\alpha_p(t)$ given by Eq. (48); Δp=0.125 r.l. (Ref. 157).

shower. The average accuracy of measuring the summed paths is 0.2. A detailed analysis of the corresponding methodological questions is given in Ref. 174.

In order to answer the question of to what degree the quantity $\Delta\Sigma r(t,p|E_\gamma)/\Delta t\Delta p$ reflects the ionization energy losses of shower electrons $\Delta\Sigma E(t,p|E_\gamma)/\Delta t\Delta p$, the Monte Carlo method was used to numerically model the ratio

$$\eta(t,p|E_\gamma)=\Delta\Sigma E(t,p|E_\gamma)/\Delta\Sigma r(t,p|E_\gamma) \tag{46}$$

for showers generated by gamma quanta of energy E_γ=100–3000 MeV in liquid xenon.[157] Two simplified probabilistic EPS models were considered, and in both cases four basic elementary processes were taken into account: electron–positron pair production, bremsstrahlung, ionization losses, and multiple Coulomb scattering. The difference between the models was that the bremsstrahlung was simulated differently in them, as a result of which one of the models (model 2) leads to a harder and at the same time more realistic (than in model 1) spectrum of shower photons and electrons.[7)] Two values were taken for the photon cutoff energy E_c, 2 and 10 MeV, and for electrons $E_c=(0.9+x)$ MeV, where x is a random quantity from the uniform distribution in the interval 0–1. This form of E_c to a large degree reflects the measurement conditions. The numbers N_γ of modeled events were selected such that the relative error $\delta\eta/\eta$ in (46) is less than 3%, at least in half the cells $\Delta t\Delta p$ of the grid (see Fig. 12). Some results of the modeling are given in Figs. 13–17 and in Table IX.

Therefore, in Fig. 13 we show the distribution of the quantity

$$\alpha(t)=\sum_p \eta(t,p|E_\gamma) \tag{47}$$

in the development length t of showers generated by gamma quanta with energy 100, 200, 500, and 1000 MeV. There we also give the values of the photon cutoff energy (model 1). The analogous distributions but for $\eta(t,p|E_\gamma)$ a summed over p only in a band of width Δp adjacent to the shower axis, i.e.,

$$\alpha_p(t)=\sum_{p\in\Delta p} \eta(t,p|E_\gamma), \tag{48}$$

are shown in Fig. 14 (Δp=0.125 r.l.) and Fig. 15 (Δp=0.375 r.l.). The dependence of

$$\alpha_t(p)=\sum_{t\in\Delta t} \eta(t,p|E_\gamma) \tag{49}$$

on the distance p from the shower axis in layers of liquid xenon of thickness Δt=0.5 r.l. for several values of t and the same values of E_γ is shown in Fig. 16. The analogous dependence is shown in Fig. 17 but for E_γ=2000 and 3000 MeV, and here the results of the two models are compared. In Table IX we give the values of the coefficient $\eta(t,p|E_\gamma)$ a averaged over the entire (t,p) plane, i.e.,

$$\bar{\eta}(E_\gamma)=\sum_{t,p} \eta(t,p|E_\gamma), \tag{50}$$

TABLE IX. Values of $\bar{\eta}(E_\gamma)$, defined by Eqs. (50) and (46), calculated according to two models of showers produced in liquid xenon by gamma quanta of energy E_γ. The shower electron cutoff energy is E_c=2 MeV, $\bar{\eta}(E_\gamma)$ is given in MeV/r.l., N_γ is the number of modeled EPS events, and $\delta\bar{\eta}(E_\gamma)\approx$0.1 (Ref. 157).

N_γ, MeV	100	200	500	1000	2000	3000	all
Model 1	12,5 640	12,9 420	13,2 200	13,2 100	13,2 55	13,4 20	13,1 1435
Model 2	13,6 448	13,6 294	13,6 140	13,6 70	13,4 40	13,6 21	13,5 1013

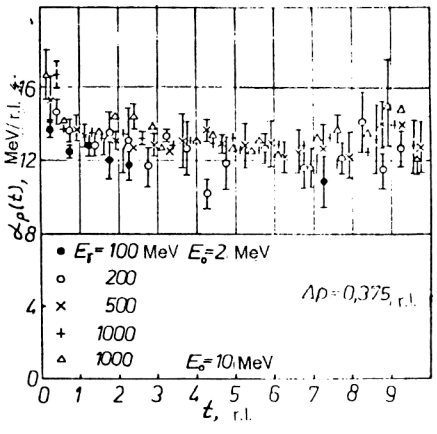

FIG. 15. The same as in Fig. 13 for $\alpha_p(t)$ given by Eq. (48); $\Delta p = 0.375$ r.l. (Ref. 157).

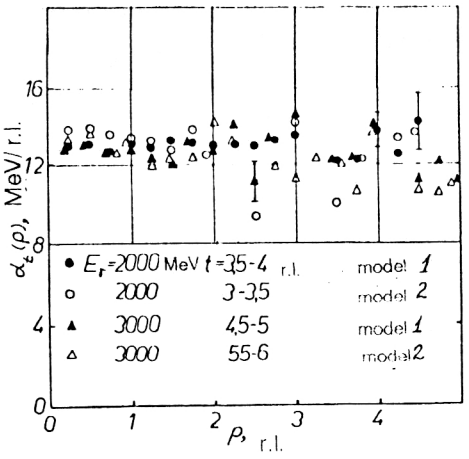

FIG. 17. The same as in Fig. 16 for other values of E_γ. The results were obtained using two models.[157]

and calculated using the two EPS models considered. There we also give the numbers N_γ of simulated cases of EPSs.

The main conclusions following from the results of modeling $\eta(t,p|E_\gamma)$ are the following.[157]

1. The projection of the summed paths of the shower electrons $\Delta\Sigma r(t,p|E_\gamma)/\Delta t\Delta p$ on the (t,p) plane in which the shower axis lies (see Fig. 12) is, with an accuracy of several percent, directly proportional to the ionization energy losses of shower electrons, at least in the central region of the shower, which contains, on the average, at least 90% of its total energy.

2. The slight increase of $\eta(t,p|E_\gamma)$ above its average value is observed only near the primary gamma-quantum conversion point, i.e., for $t \lesssim 1$ r.l. and $p \lesssim 0.1$ r.l. (see, for example, Figs. 11 and 15), and is due to the fact that in this part of the shower the ionization energy losses of electrons with $E \simeq E_\gamma/2$ are maximal, and the length of the projection of their tracks is minimal on the average.

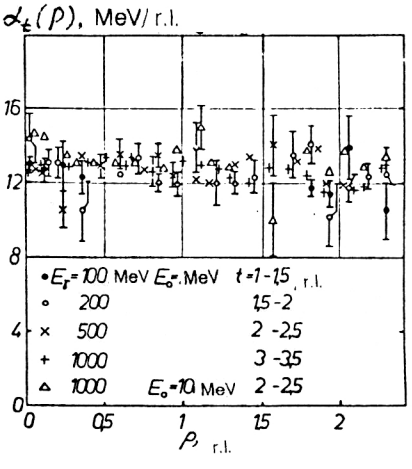

FIG. 16. Dependence of $\alpha_p(t)$ given by Eq. (49) on the distance p from the axis of showers produced in liquid xenon by gamma quanta of energy E_γ. E_0 is the shower photon cutoff energy used in the modeling. The ranges of depths t to which the corresponding distributions refer are given.[157]

3. The quantity $\eta(t,p|E_\gamma)$ decreases, according to model 1, with increasing t within $\sim 10\%$ outside this central region of the shower. However, according to model 2 this falloff is considerably smaller. In addition, a decrease of $\eta(t,p|E_\gamma)$ with increasing p at sufficiently large distances from the shower axis is not observed.

4. The numerical values of $\bar{\eta}(E_\gamma)$ averaged over the entire observation plane (t,p) satisfactorily agree with the analogous results obtained in the modeling of showers by the MC method for lead glass.[29]

A detailed analysis of $\eta(t,p|E_\gamma)$ is made in Ref. 175. In Refs. 38, 149, 158, 162, and 166–173 it is assumed that $\eta(t,p|E_\gamma)$ is constant. We also note that the accuracy of determining the gamma-quantum energy E_γ in the XBC is $\Delta E_\gamma/E_\gamma \lesssim 0.1$ if the showers produced by these gamma quanta develop completely inside the recording volume of the chamber.[142] The fundamental information about the experimental data used in the studies discussed below (Refs. 149 and 168–173) is given in Table X. These data were obtained by scanning 220 thousand photographs of the 180-liter XBC at ITEP (Moscow), bombarded by a beam of π^- mesons with momentum 3.5 GeV/c.

The longitudinal shower development

A typical example of the longitudinal distribution of the energy deposition in showers produced in lead, copper, and aluminum by electrons of energy 6 GeV is shown in Fig. 18 (Ref. 73). There we also show the corresponding results from the Monte Carlo modeling. This example has recently come to be considered a classic and is cited in monographs on high-energy physics and particle detectors (Refs. 75, 117, and 132). In Fig. 19 we show the analogous distributions obtained for gamma quanta of energy $E_\gamma = (175 \pm 15)$, (455 ± 45), (1125 ± 125), (2115 ± 125), (3125 ± 125), and (3375 ± 125) MeV, initiating showers in liquid xenon.[172] The experimental data are described satisfactorily by a Weibull distribution, at least to the shower development depth t at which the energy deposition over a single radiation length falls to $\sim 0.1\%$. The Weibull distri-

TABLE X. Basic information about the experimental data used in Refs. 149 and 168–173: E_γ is the energy of the gamma quantum producing the shower, ΔE_γ is the width of the interval, $\bar{E}_\gamma$ is the average shower energy in a given interval, N_γ is the number of showers selected in the scanning which satisfy the first two criteria, $L_{\min}$ is the minimum potential development length according to the third criterion, and N_γ^* is the number of showers satisfying all three criteria.[149]

$E_\gamma \pm \Delta E_\gamma$, MeV	$\bar{E}_\gamma$, MeV	N_γ	$L_{\min}$, r.l.	N_γ^*
3375±125	3489±35	46	24,0	15
3125±125	3139±18	42	24,0	12
2875±125	2850±17	41	24,0	11
2625±125	2599±25	53	22,6	12
2375±125	2373±16	60	22,6	20
2125±125	2117±15	63	21,3	35
1875±125	1864±12	80	20,5	33
1625±125	1615±9	108	20,0	66
1375±125	1363±10	129	20,0	58
1125±125	1116±8	158	20,0	80
875±125	871±8	204	20,0	86
680±70	677±5	138	20,0	60
555±55	555±4	108	20,0	58
455±45	459±3	103	18,6	59
375±35	380±3	65	17,3	61
310±30	309±2	58	16,0	53
255±25	252±2	55	14,9	55
210±20	208±2	49	14,8	47
175±15	177±2	29	12,6	29
145±15	145±2	24	12,6	24
120±10	123±2	21	11,6	20
100±10	100±1	23	11,0	14
Over all energies		1657		908

bution was first used by Barylov, Demidov *et al.* to reconstruct the total shower energy when the layer of active matter—liquid xenon in a XBC—has finite thickness.[176] The same distributions but in the quantity $x = t/\bar{t}(E_\gamma)$ are shown in Fig. 20. Here $\bar{t}(E_\gamma)$ is the average shower development length, the energy dependence of which is shown in Fig. 21 and is approximated by Eq. (35). We note that for $E_\gamma \gtrsim 500$ MeV and $x \gtrsim 0.15$ these distributions do not

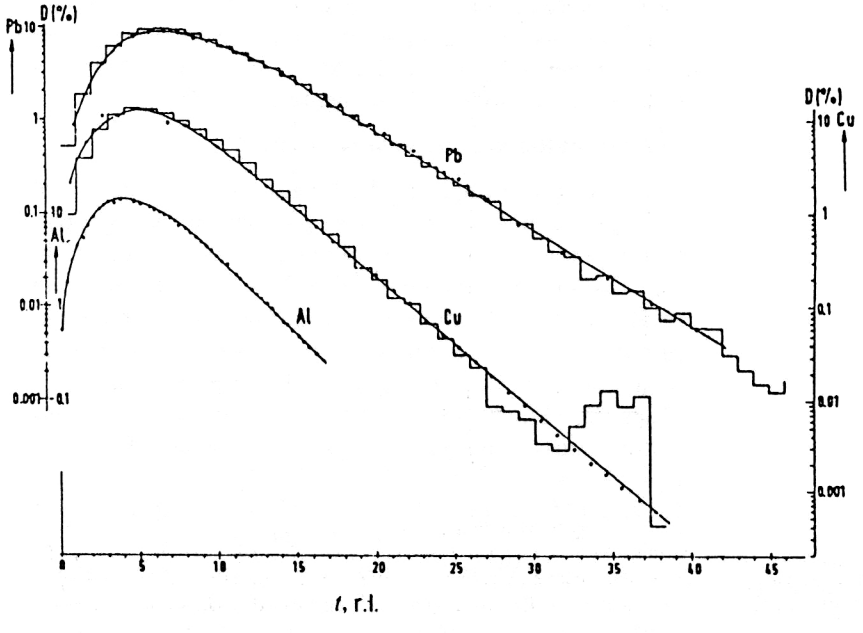

FIG. 18. Longitudinal distribution of the dose D (in %) in showers produced by 6-GeV electrons in lead, copper, and aluminum.[73] The histograms are the result of Monte Carlo modeling.

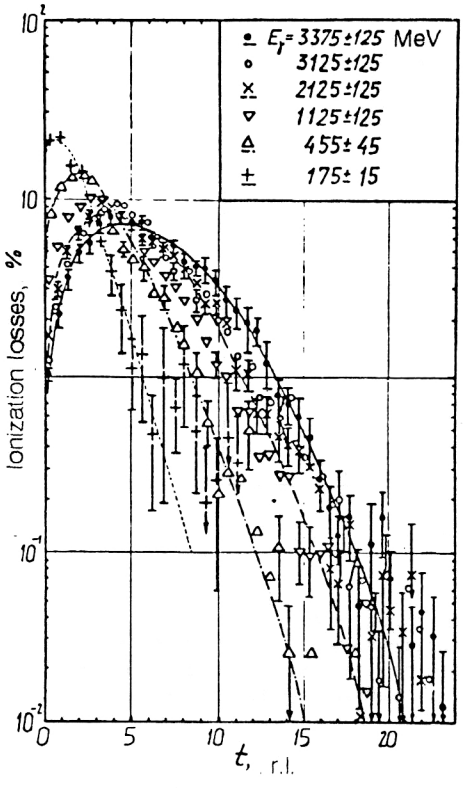

FIG. 19. Longitudinal distribution of average ionization energy losses in showers produced by gamma quanta with energy E_γ in liquid xenon.[172] The curves show the corresponding approximating functions as Weibull distributions.

differ from each other within the experimental error. This conclusion was arrived at in Ref. 149 on the basis of analysis of the longitudinal distributions of showers from all 22 intervals of E_γ studied, six of which are shown in Fig. 20. Therefore, there are grounds for summing these distributions over the energy E_γ in this interval, i.e., from 500 to 3500 MeV. In this case such a summation implies only averaging over fluctuations. The result is shown in Fig. 22. There we show the function

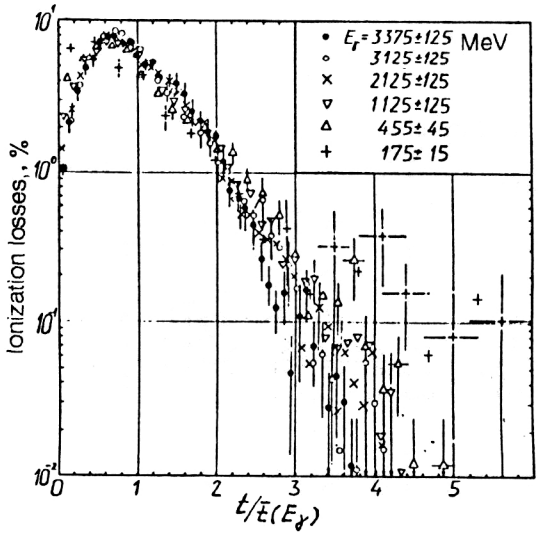

FIG. 20. The same as in Fig. 19 for the dimensionless development length $t/\bar{t}(E_\gamma)$, where $\bar{t}(E_\gamma)$ is the average development length of a shower with energy E_γ (Ref. 149).

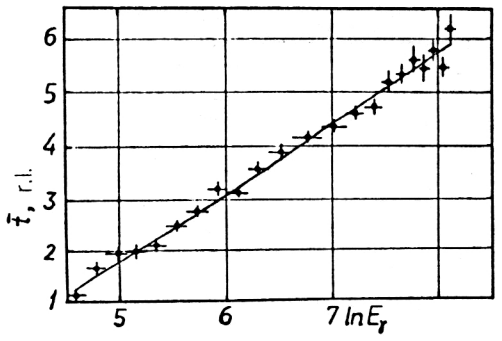

FIG. 21. Dependence of the average development length of a shower produced in liquid xenon on the primary gamma-quantum energy E_γ. The straight line shows the approximating function (35) (E_γ is in MeV).

$$F_1(x)=a_1x^{a_2}\exp(-a_3x), \tag{51}$$

describing the experimental data. The parameters a_i ($i=1,2,3$) selected in the fit are $a_1=83.1\pm3.4$, $a_2=1.65\pm0.03$, and $a_3=2.62\pm0.03$, and $\chi^2/35=35.8$ for $x\gtrsim0.15$ (Ref. 149). At small values of the development length ($x\lesssim0.15$) one can observe a systematic decrease in the ionization energy losses (Fig. 20) due to the dependence of multiple Coulomb scattering on the energy of the electrons appearing at the very beginning of the shower. We note that this effect will be observed only when the conversion point of the gamma quantum generating the shower is clearly fixed. The function $F_1(x)$ is normalized

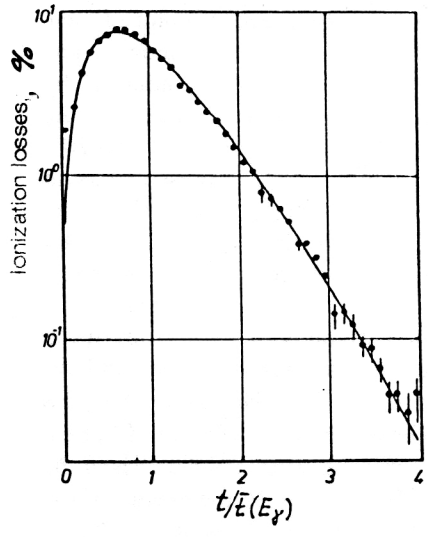

FIG. 22. Longitudinal distribution of ionization energy losses in showers produced by gamma quanta in liquid xenon, averaged over the energy of the primary gamma quantum E_γ; $\bar{t}(E_\gamma)$ is the average shower development length. The averaging is performed over the interval E_γ=500–3500 MeV (Ref. 149).

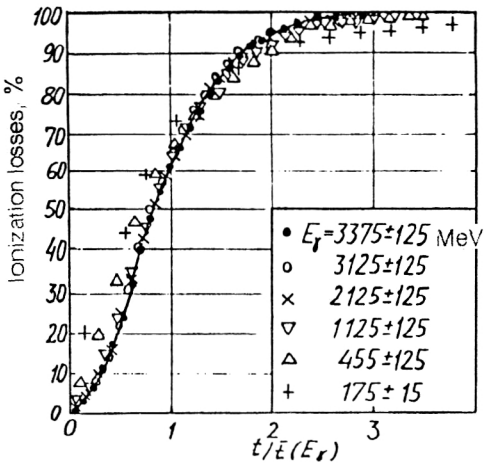

FIG. 23. The same as in Fig. 19 in the form of integrated distributions and as a function of the ratio $t/\bar{t}(E_\gamma)$ (Ref. 149). The solid line shows the accumulated probability function obtained from Eq. (51).

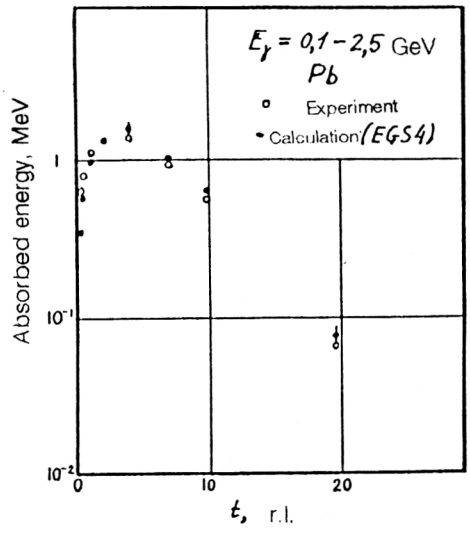

FIG. 24. Longitudinal distribution of the absorbed energy of showers produced by bremsstrahlung photons of energy from 100 MeV to 2.5 GeV in lead.[61] The experimental data are compared to the results of EPS modeling by the Monte Carlo method using the EGS-4 program.

to unity. It should be emphasized that it has the same form as the weight function (27) and the distribution (40) approximating the results of shower modeling by the MC method. However, here it is expressed in terms of the dimensionless shower development length $x=t/\bar{t}(E_\gamma)$. From this we can conclude that the average shower development length $\bar{t}(E_\gamma)$ is a suitable scale parameter for removing the energy dependence of the average longitudinal energy-deposition profiles in showers (see, for example, Ref. 19). Naturally, it also contains information about the properties of the material in which the shower develops (for amorphous and homogeneous media) and about the cutoff energy of the shower particles. Information about the shower observation conditions (the number of shower electrons, the mean free path, the light or scintillation effect) is mainly contained in the normalization factor a_1 (51).

Of particular interest from the practical point of view is the integrated energy-deposition profile in a shower. The corresponding distributions for showers induced by gamma quanta in liquid xenon are given in Fig. 23 (the values of the energy E_γ are the same as in Figs. 19 and 20). The solid line shows the function (51), respresented as an accumulated probability distribution $\int_0^x F_1(x')dx'$. It may be noted that, for example, more than 90% of the total shower energy is absorbed in matter of thickness $\sim 2\bar{t}(E_\gamma)$.

The experimental data pertaining to showers produced by monoenergetic gamma quanta are very sparse and have mainly been obtained using XBCs. However, the EPS characteristics have also been studied in a beam of bremsstrahlung photons, the energy spectrum of which lies in the range from 100 to 2500 MeV, i.e., up to the energy of the beam of emitting electrons.[61] In Fig. 24 we show the distribution of energy absorbed in the scintillator from showers produced by such photons in lead as a function of the thickness of the layer of lead in front of the scintillator. The experimental data are compared to the results of calculations performed by the MC method using the EGS-4 program,[26] where it is assumed that the cutoff energy is 0.1 MeV for photons and 1 MeV for electrons. The authors conclude that there is agreement to within 16%, except for the two first points at the lead thickness equal to 1 and 2 mm (Ref. 61).

The longitudinal shower profile has been studied in beams of electrons of energy up to 200 GeV (Ref. 86). Some of the first experimental data besides those mentioned earlier[73] pertained to the energy range $E=2$–15 GeV of the primary electrons producing showers in lead.[72] These data are given in Fig. 25 together with the approximating curves obtained in Ref. 72. The threshold energy of the shower electrons is 7.4 MeV. We see from this figure

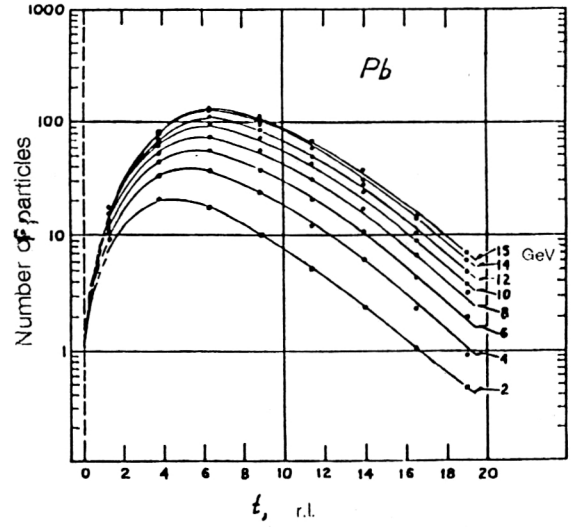

FIG. 25. Longitudinal profiles of showers produced in lead by electrons of energy 2–15 GeV (values given on the figure; Ref. 72). The approximating function is shown by the solid lines.

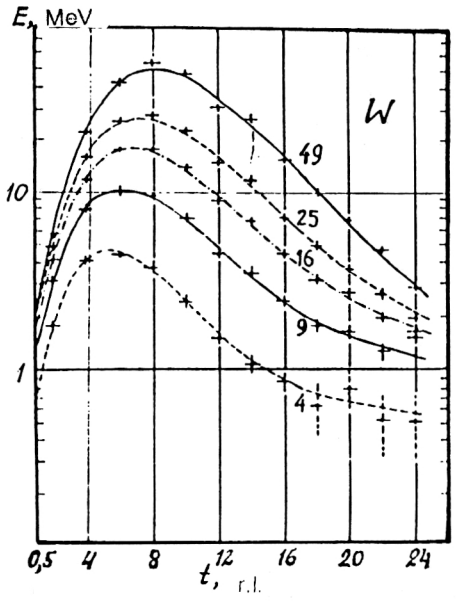

FIG. 26. Longitudinal development of showers produced by electrons of energy 4, 9, 16, 25, and 49 GeV in the Si/W sandwich calorimeter.[81,82] The approximating curves (52) are shown by the lines.

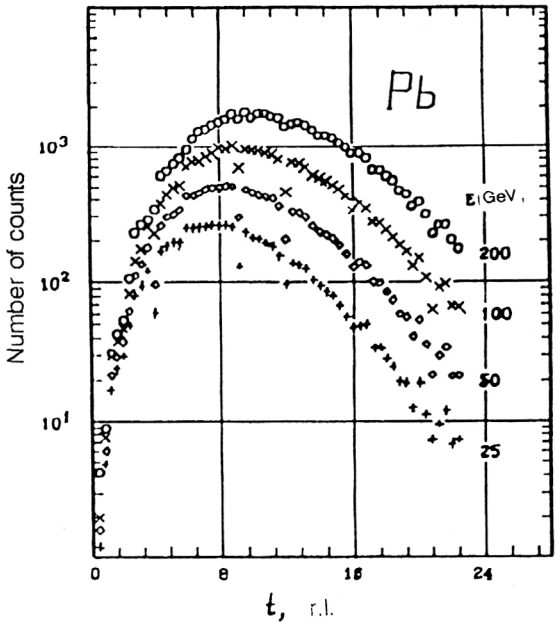

FIG. 27. Longitudinal profiles of showers produced by electrons of energy 25, 50, 100, and 200 GeV in lead.

that, as in the case of the other experimental data on the longitudinal development of EPSs, near the shower maximum the average profile of the shower rather rapidly reaches the asymptotic form of dependence on the development length t, i.e., exponential decrease with increasing t (see also Figs. 18–20). Nevertheless, in studies of the longitudinal development of showers generated by electrons with energy from 4 to 49 GeV in the Si/W sandwich calorimeter a more complicated dependence of the EPS profile on t has been observed in the asymptotic region.[81,83] The corresponding data are shown in Fig. 26. There we also give the approximating curves, which, in the opinion of the authors of Ref. 81, describe the experimental results better than Eq. (40). These curves show the two-component distribution:[81]

$$E=E_0(t/2)^a\exp(-bt)+E_1(t/2)^c \times\exp[-m(t-x_1)-y_1], \qquad (51')$$

where E, E_0, and E_1 are in MeV; c, m, x_1, and y_1 are dimensionless constants selected in the fit with

$$a=(3.2\pm0.5)+(0.3\pm0.2)\ln E,$$

$$b=(0.75\pm0.10)+(-0.05\pm0.04)\ln E,$$

$$c=(0.26\pm0.10)\ln E, \quad m=(0.04\pm0.02)\ln E,$$

$$x_1=(-6.8\pm3.5)+(55.9\pm20.3)\ln E,$$

$$y_1=2.5\pm0.4,$$

$$E_0=(2.2\pm1.2)+(1.5\pm0.6)\ln E \ [\text{MeV}],$$

and $\chi^2/49=48$. It is interesting that a similar two-component form of the energy-deposition profile has been observed also in hadron showers generated by pions of energy 10 and 30 GeV (Refs. 178 and 179). However, some recent measurements of the longitudinal profiles of showers produced by electrons of energy 25, 50, 100, and 200 GeV in a highly segmented electromagnetic calorimeter[86] most probably do not confirm the model of the two-component structure (51'). The results of the measurements are given in Fig. 27.

Transverse shower development

As characteristics of the transverse development of a shower it is usual to take the radial (i.e., in the direction perpendicular to the shower axis) distribution of the energy deposition observed at a given length (depth), measured from the start of the shower along the shower axis, or summed over the entire shower development depth. The experimental data pertaining to the transverse profiles of showers are most often approximated by a two-component function (Refs. 59, 73, 78, 82, 83, and 88):

$$F_1(r,t)=c_1\exp[-r/\lambda_1(t)]+c_2\exp[-r/\lambda_2(t)], \qquad (52)$$

although some authors prefer the usual exponential distribution.[80] Here the constants c_1 and c_2 and also the t dependence of the slope parameters $\lambda_1(t)$ and $\lambda_2(t)$ are determined from the measurement results. The physical interpretation of the model (52) is that in the transverse direction in a shower two regions can be distinguished: a central region characterized by relatively small angular spread of the hard component of the shower particles due mainly to the insignificant angular dependence of bremsstrahlung processes and electron–positron pair production [this region is described by the first term in (52)], and the peripheral region containing mainly low-energy particles undergoing strong multiple Coulomb scattering [second

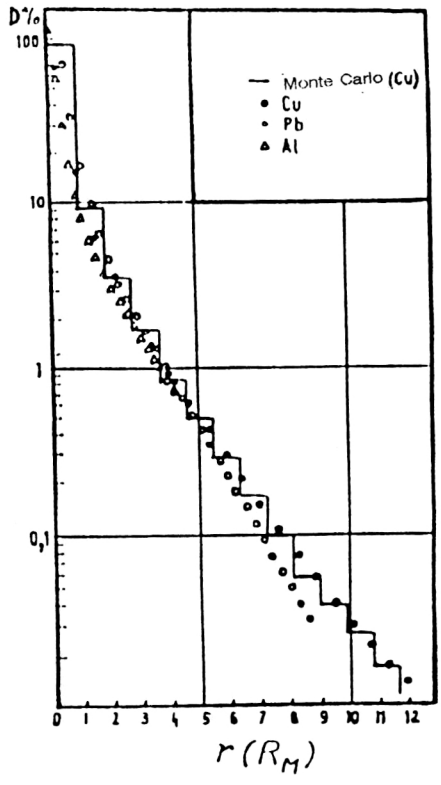

FIG. 28. Transverse distribution of the energy deposition in showers produced by 6-GeV electrons in copper, lead, and aluminum.[73] The results of the Monte Carlo calculations are shown by the histogram. The distributions are summed over the entire shower development depth. r is the distance from the shower axis, expressed in Molière units (22).

term in (52)]. The photographs of showers recorded in XBCs can serve as a clear illustration of this interpretation (Figs. 1, 2, and 8). We also see that $\lambda_1(t)$ and $\lambda_2(t)$ must grow with the development depth t.

The results of dosimetry measurements of the transverse distributions of showers produced by electrons of energy 6 GeV in copper, lead, and aluminum are shown in

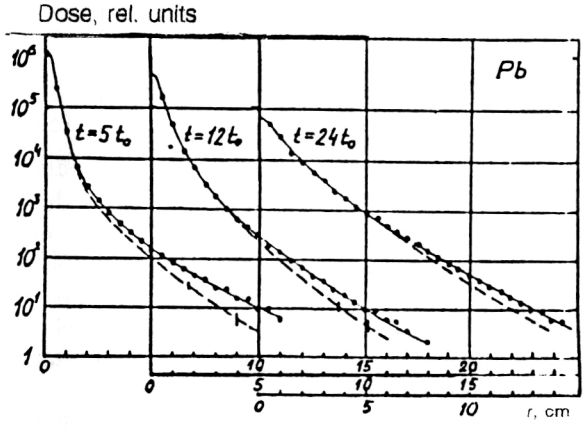

FIG. 29. Transverse profiles of the energy deposition in showers produced by 6-GeV electrons at the three indicated values of the shower development depth t in lead ($t_0=1$ r.l.; Ref. 73). r is the distance from the shower axis. The dashed lines show the Monte Carlo calculation.

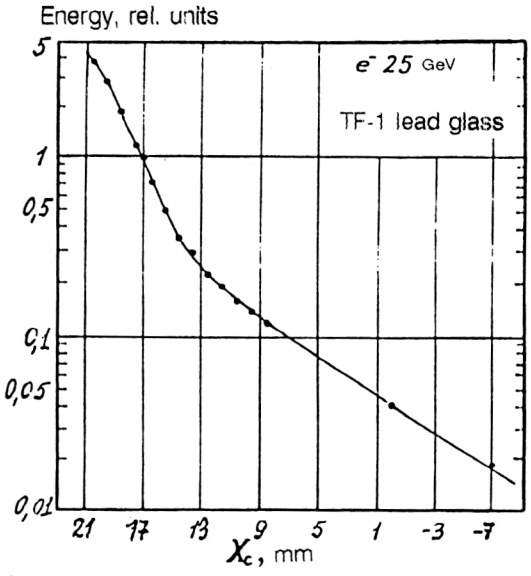

FIG. 30. Radial distribution of energy deposited in showers produced by 25-GeV electrons in lead glass.[78] The curve shows the parametrization (52) with $\lambda_1=4.5$ mm, $\lambda_2=12$ mm, and $c_1/c_2=0.14$.

Fig. 28. These distributions are summed over the entire development depth. The experimental data are compared to the results of the calculation using the Monte Carlo model. The authors also measured the corresponding distributions at certain values of the depth t in aluminum and lead. The distributions for lead are reproduced in Fig. 29. We see that, at least at relatively small depth ($t=5$ r.l.) a

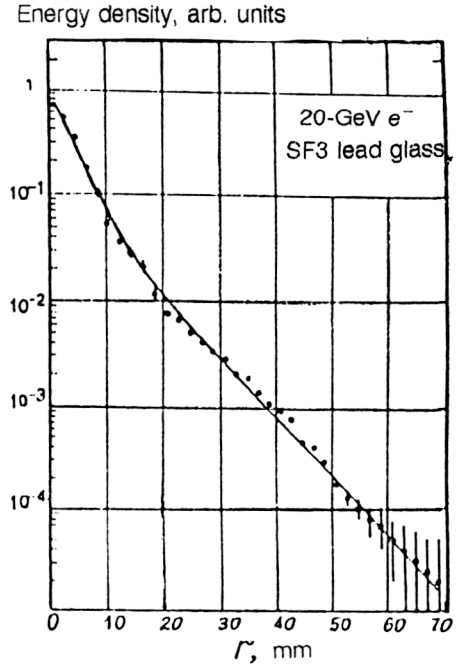

FIG. 31. The same as in Fig. 30, but for 20-GeV electrons.[82] The parameter values are $\lambda_1=(3.4\pm0.1)$ mm, $\lambda_2=(9.3\pm0.3)$ mm, and $c_1/c_2=11.9\pm0.5$.

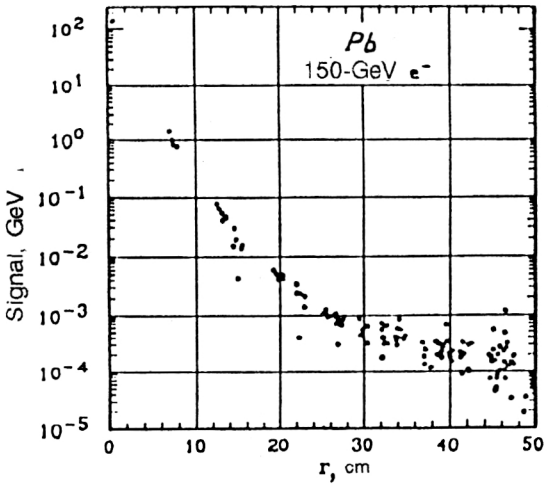

FIG. 32. Transverse profiles of showers produced by 150-GeV electrons in a "spaghetti"-type calorimeter.[87]

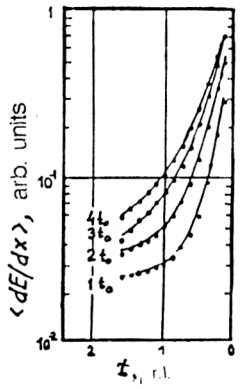

FIG. 33. Radial distribution of the average charge in showers produced by 3-GeV electrons in lead glass at the indicated values of the development depths ($t_0=1$ r.l.; Ref. 59).

two-component shower structure can be seen and that as the development depth increases the shower becomes more and more uniform in this respect. The change of the regime of transverse shower development can be seen very clearly from the data of Ref. 78, where the radial dependence, summed over the depth, of the energy deposition in showers produced in lead glass by electrons of energy 25 GeV was measured. The authors describe the experimental data (Fig. 30) by the function (52) with $c_1/c_2=0.14$, $\lambda_1=4.5$ mm, and $\lambda_2=12$ mm (Ref. 78). Analogous results were obtained in calibrating the front part of the electromagnetic spectrometer of the DELPHI detector in a 20-GeV electron beam (Ref. 82). They are shown in Fig. 31 together with the parametrizing function (52), where $c_1/c_2=11.9\pm0.5$, $\lambda_1=(3.4\pm0.1)$ mm, and $\lambda_2=(9.3\pm0.3)$ mm, for $\chi^2=2.6$. The transverse profiles of showers produced by electrons of energy 150 GeV were also measured by a fine-grained, lead–scintillating fiber calorimeter (Fig. 32; Ref. 87). Here a two-component structure of the form (52) is seen, although the authors have not parametrized their data. We also give the results of the measurement of the transverse charge distribution at various depths of showers produced by 3-GeV electrons in lead glass (Fig. 33; Ref. 59). As before (Fig. 29), it may be noted that with increasing shower development depth the transverse profile of the shower is described more and more accurately by an exponential function.

The two-component parametrization of the transverse profile of showers produced by electrons of energy 2, 4, and 6 GeV in tungsten and uranium has been discussed in Ref. 84, where the experimental results were described by the function

$$F(r)=[\exp(-\sqrt{r/\lambda_1})+c_{12}(\exp(-r/\lambda_2)]/(Nr), \tag{53}$$

where N, c_{12}, λ_1, and λ_2 are parameters determined from the experimental data as in Eq. (52). It was concluded that the attenuation parameter λ_2 is nearly independent both of the depth t and of the primary electron energy E, while λ_1 is proportional to t and $E^{-1/2}$ and is the same for the two absorbers.[84] It is also amusing to note that a two-component structure is observed also in the transverse profiles of hadron showers produced by pions and protons of momentum 1.56, 2.46, 5.65, and 6.80 GeV/c in a segmented (lead–scintillator) calorimeter.[180] The experimental data are satisfactorily described by a function of the form (52) for primary pions and protons with momentum beginning at least at 2.46 GeV/c and above.

A detailed experimental study of the transverse structure of showers produced by gamma quanta of energy from 100 to 3500 MeV in liquid xenon has been carried out using the XBC (Refs. 38, 149, 172, and 173). The method of study and the general features of the experimental data obtained have been described above. Here we give the main results.

As an example, in Figs. 34a and 34b we show the two-dimensional, i.e., in the shower plane (t,p), distributions of ionization energy losses of shower electrons in EPSs produced by gamma quanta with energy $E_\gamma=(555\pm55)$ and (2125 ± 125) MeV (see Fig. 12). The dashed lines show the approximating curves

$$f(p\,|\,t,E_\gamma)=\exp[-p/\bar{p}(t,E_\gamma)]/\bar{p}(t,E_\gamma), \tag{54}$$

where $\bar{p}(t,E_\gamma)$ is the slope parameter depending on the shower development depth and the energy E_γ. This is the only parameter selected in the fit of the experimental data. The t dependence of this parameter for all 22 studied ranges of the energy E_γ is reproduced in Fig. 35. It is approximated by the linear function[173]

$$\bar{p}(t,E_\gamma)=\alpha+\beta(E_\gamma)t, \tag{55}$$

which is also shown in these figures. Here the coefficient is $\alpha=(0.042\pm0.015)$ r.l. and is independent of E_γ within the error. The energy dependence of the coefficient $\beta(E_\gamma)$ is shown in Fig. 36 and parametrized by the function[173]

$$\beta(E_\gamma)=a+b\ln E_\gamma \tag{56}$$

in the range $E_\gamma\gtrsim175$ MeV. The values of the constants are given in Table XI for various ranges of t (β is a dimensionless quantity and E_γ is in MeV).

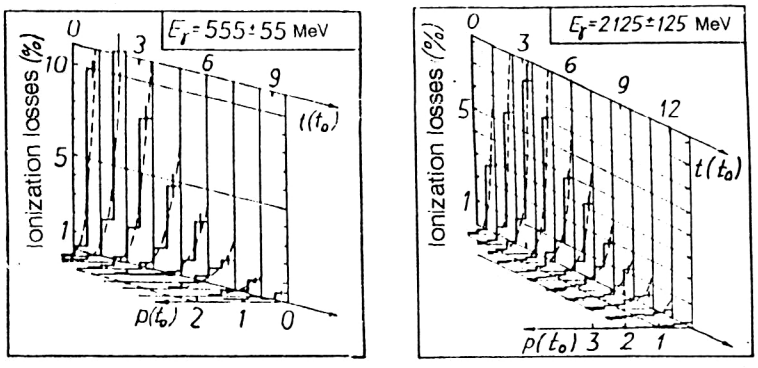

FIG. 34. Two-dimensional distribution of ionization losses in showers produced in liquid xenon by gamma quanta of energy (a) $E_\gamma = (555 \pm 55)$ MeV and (b) $E_\gamma = (2125 \pm 125)$ MeV (Ref. 149); t is the development length and p is the distance from the shower axis in the plane of the photograph ($t_0 = 1$ r.l.). The approximating curves (54) are shown by the dashed lines.

The transverse profiles, summed over development depth, of showers produced in liquid xenon by gamma quanta of energy E_γ in seven ranges of values from 100 to 3500 MeV are shown in Fig. 37. These profiles were measured in the plane of the photograph (the plane of the shower axis). The energy dependence of the average widths $\bar{p}_0(E_\gamma)$ of the profiles pertaining to all 22 of the ranges of E_γ studied are shown in Fig. 38. There we also show the parametrization of this dependence by the function[172]

$$\bar{p}_0(E_\gamma) = a_p + b_p \ln E_\gamma , \qquad (57)$$

where E_γ is in MeV, $a_p = (0.21 \pm 0.03)$ r.l., and $b_p = 0.085 \pm 0.005$.

If the width p is normalized to the average width $\bar{p}_0(E_\gamma)$ as in the case of longitudinal shower development (Fig. 20), it turns out that the average shower profiles determined in the plane of the shower axis cease to depend on the energy E_γ of the primary gamma quanta at $E_\gamma \gtrsim 500$ MeV (Fig. 39). One can therefore conclude, like before, that the average width $\bar{p}_0(E_\gamma)$ is a suitable scaling parameter which unifies the longitudinal shower profiles, summed over depth, in the plane of the shower axis in this range of E_γ.

Using the relation taking into account the conditions under which showers in the XBC were photographed and the axial symmetry (on the average) of the showers, we can reconstruct the radial density of the ionization losses $F_r(r|t,E_\gamma)$ (Ref. 152):

$$f(p|t,E_\gamma) = 2\int_p^\infty F_r(r|t,E_\gamma)\,dr/\sqrt{1-(p/r)^2}\,, \qquad (58)$$

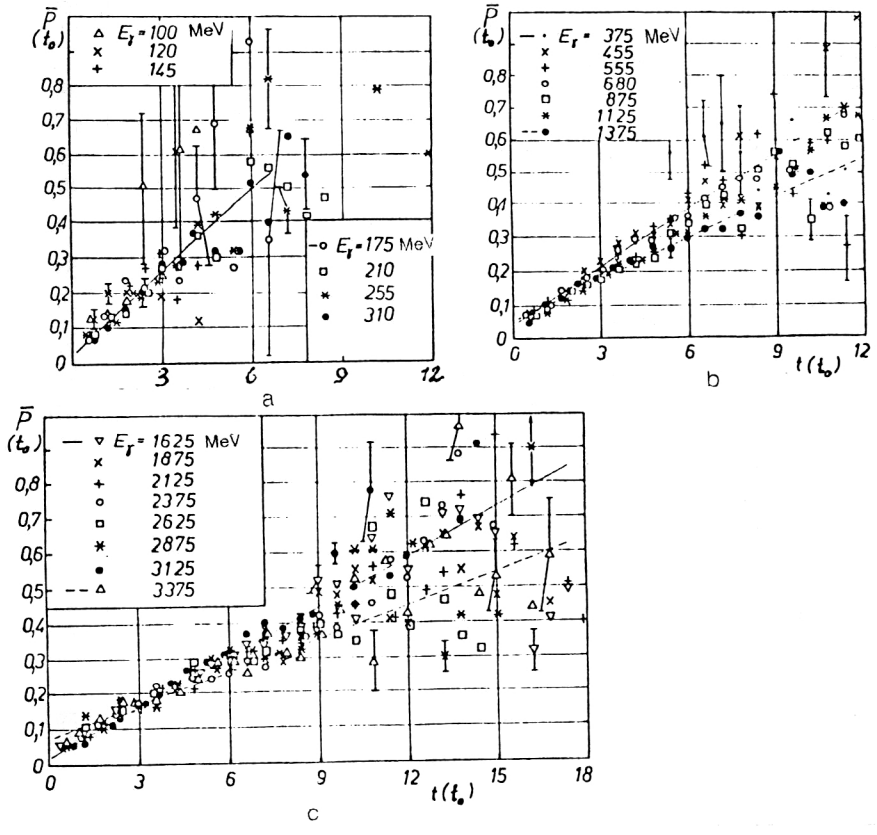

FIG. 35. Dependence on the shower development depth t of the slope parameter $\bar{p}(t,E_\gamma)$ of the function (54) for various values of the energy E_γ of the gamma quanta initiating showers in liquid xenon.[149] The approximating functions (55) are shown by the straight lines.

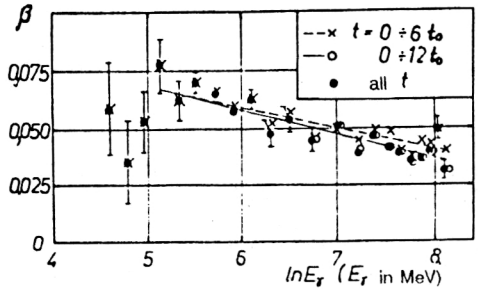

FIG. 36. Energy dependence of the coefficient β in Eq. (55) (Ref. 173). The solid and dashed lines show the approximating function (56) for the two given ranges of t ($t_0=1$ r.l.).

where r is the distance from the shower axis. The solution of this integral equation has the form[152]

$$F_r(r|t,E_\gamma)=[1/(\pi r^2)]\int_\infty^r \frac{d}{dp} \times[pf(p|t,E_\gamma)]dp/\sqrt{1-(r/p)^2}. \quad (59)$$

The final expression for the radial profile function of a shower is obtained by substituting (54) into (59). Here we introduce the following notation: $s=r/p$, $x=r/\bar{p}(t,E_\gamma)$, and

$$F(x)=\pi\bar{p}^2(t,E_\gamma)F_r(r|t,E_\gamma). \quad (60)$$

Then[181]

$$F(x)=\int_0^1 (1/s-1/x)/[s^2\sqrt{1-s^2}]\exp(-x/s)ds. \quad (61)$$

The function $F(x)$ depends only on the dimensionless radius x. Therefore, the average radial profile of the ionization energy losses in showers produced in liquid xenon by gamma quanta of energy $E_\gamma=500$–3500 MeV can be expressed in terms of the universal function $F(x)$ and the average width $\bar{p}(t,E_\gamma)$ of the shower at depth t:

$$F_r(r|t,E_\gamma)=[\pi\bar{p}^2(t,E_\gamma)]^{-1}F(x). \quad (62)$$

It has been shown that at large x ($x\gtrsim 2$) $F(x)\sim\exp(-x)$ (Ref. 181), in complete agreement with other experimental data. The function $F(x)$ is shown graphically in Fig. 40. We see that at small x, i.e., when $r\lesssim\bar{p}$ and, consequently, the function $F(x)$ describes the radial distribution near the shower axis, its x dependence is stronger. But if here $\bar{p}\lesssim 1$ r.l., we are dealing with the central region of the shower, as discussed above. It is also easy to see that at the start of the shower ($\bar{p}<1$ r.l.) the central region dominates on the average, and as the development depth increases there is a smooth transition to the regime of stronger transverse scattering of lower-energy electrons characteristic of the peripheral region. This picture completely corresponds to the available experimental data, but, in contrast to the model of the two-component structure of the transverse profiles, here there is no need to postulate two mechanisms for the scattering of shower particles.

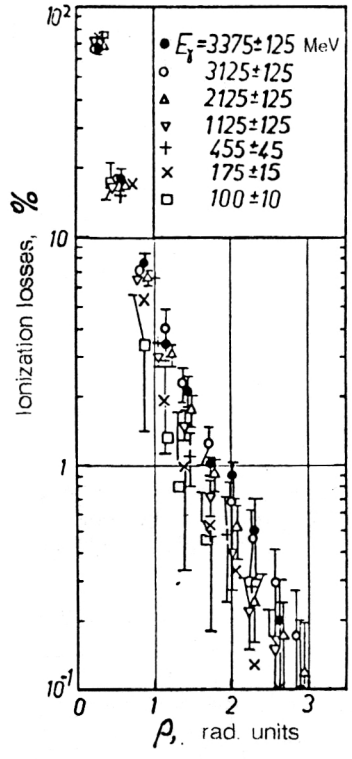

FIG. 37. Transverse profiles of showers produced in liquid xenon by gamma quanta of energy E_γ. The profiles measured in the plane of the photograph are summed over the shower development depth.[172]

Fluctuations

SInce it is the fluctuations of the energy deposition in showers which are of greatest practical interest at present, we shall not touch upon the experimental studies mentioned earlier in which fluctuations of the particle number in showers were studied, especially since these two shower characteristics are related.[29,57]

TABLE XI. Values of the parameters a and b in Eq. (56) for different depth ranges t for $E_\gamma\gtrsim 175$ MeV (Ref. 173).

t, rad. units	$a\cdot 10^3$	$-b\cdot 10^4$
0—6	67 ± 4	53 ± 5
0—12	72 ± 3	62 ± 4
Over all t	75 ± 3	66 ± 4

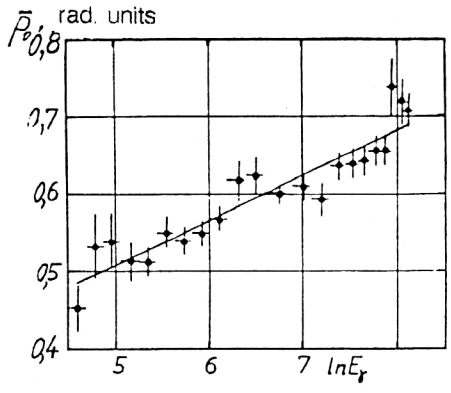

FIG. 38. Average widths of showers produced by gamma quanta of energy E_γ in liquid xenon. The measurements were made in the plane of the photograph. The approximating function (57) is shown by the solid line, and E_γ is in MeV.[172]

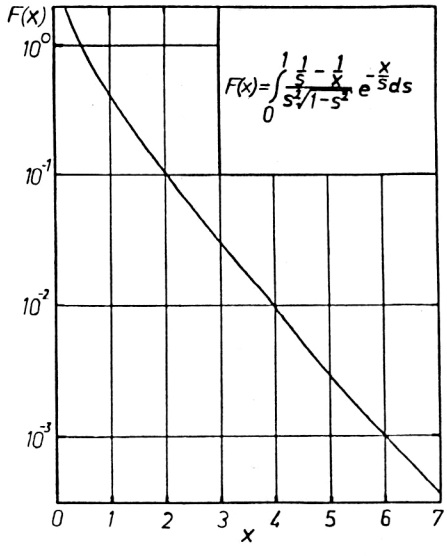

FIG. 40. Universal function of the radial shower profile $x=r/\bar{p}(t,E_\gamma)$, where $\bar{p}(t,E_\gamma)$ is the average width of a shower produced by a gamma quantum of energy E_γ, t is the shower depth, and r is the distance from the shower axis.

Longitudinal fluctuations

It is natural to represent longitudinal fluctuations of the ionization energy losses of shower electrons as the rms deviation $\sigma_A^{(t)}$ from the average fraction A of these losses ($0 \leqslant A \leqslant 1$). Let us consider the dependence of $\sigma_A^{(t)}$ on A, where the dimensionless variable A is the accumulated probability of the mean longitudinal energy deposition in the shower as a function of the depth t (51):

$$A(x)=\int_0^x F_1(x')dx', \tag{63}$$

where $x=t/\bar{t}(E_\gamma)$. This characteristic of the longitudinal fluctuations in showers was first introduced in Ref. 56. In Fig. 41 we show the dependence of $\sigma_A^{(t)}$ on A for showers generated in liquid xenon by gamma quanta of energy E_γ from 100 to 3500 MeV (Ref. 172). It has been found that for $E_\gamma \gtrsim 500$ MeV this dependence practically does not change with energy E_γ and can be approximated by the function[173]

$$\sigma_A^{(t)}=A\{[\alpha_t^2+\beta_t(\gamma_t-A)]^{1/2}-\alpha_t\}, \tag{64}$$

where $\alpha_t=(38\pm1)10^{-3}$, $\beta_t=(166\pm5)10^{-3}$, and $\gamma_t=1.01\pm0.01$. This function is shown by the solid line in Fig. 41. It is not difficult to find the dependence of $\sigma_A^{(t)}$ on the development depth from (64). For this it is necessary to change to the variable t after solving Eq. (63) for x.

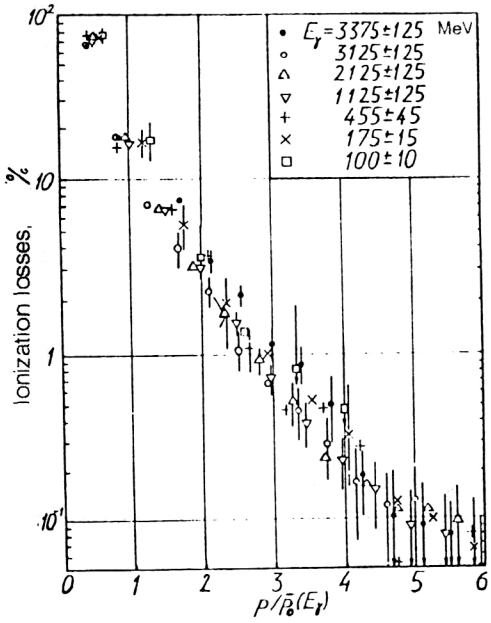

FIG. 39. The same as in Fig. 37 as a function of the dimensionless ratio $p/\bar{p}(E_\gamma)$ (Ref. 172).

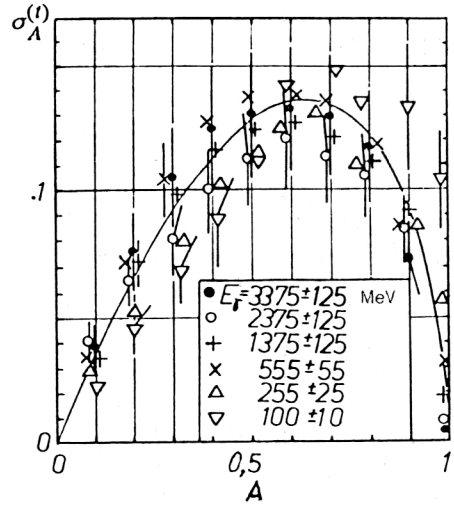

FIG. 41. A dependence of the rms deviation σ_A from the average fraction A of ionization energy losses for energy deposited along the shower axis. E_γ is the energy of the gamma quantum producing the shower in liquid xenon.[172] The approximating function (64) is shown by the solid line.

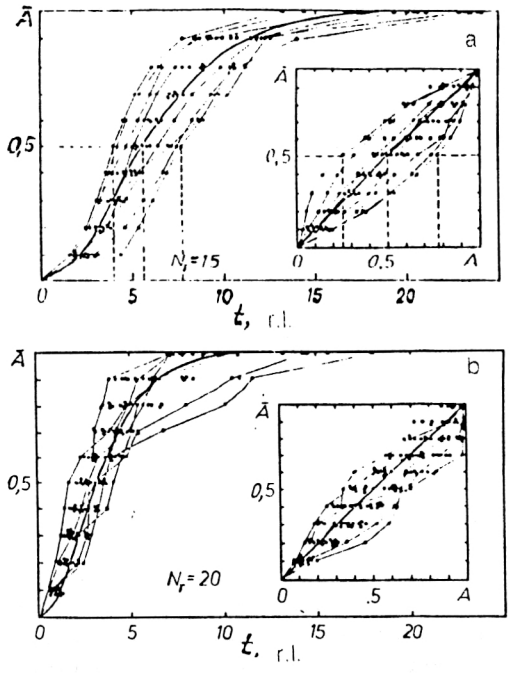

FIG. 42. Distribution of the fraction $\bar{A}$ of ionization energy losses in showers produced in liquid xenon by gamma quanta of energy (a) $E_\gamma=(3375\pm125)$ MeV and (b) $E_\gamma=(555\pm55)$ MeV (explanations given in the text).[169]

However, the representation of the longitudinal fluctuations as a dependence of $\sigma_A^{(t)}$ on A is also of practical value. For example, it may be noted (Fig. 41) that at the matter thickness in which on the average half the shower energy is deposited (i.e., $A=0.5$), the rms spread of the fraction of this energy deposition is $\sigma_A^{(t)}=0.16$, i.e., the actual energy deposition will fluctuate roughly from 0.34 to 0.66 of the total shower energy. A clear picture of the fluctuations of the longitudinal shower development is given by Figs. 42a and 42b, in which as an illustration we show the distribution in the depth t of the ionization energy losses in showers produced in liquid xenon by gamma quanta of energy $E_\gamma=(3375\pm125)$ MeV (Fig. 42a) and $E_\gamma=(555\pm55)$ MeV (Fig. 42b). These distributions are represented as the accumulated probability separately for each individual case of a shower from a sample numbering $N_\gamma=15$ and $N_\gamma=20$, respectively. The experimental points pertaining to several cases are connected by straight lines for each shower separately. The function (63) is shown by the solid line. We see that, for example, the matter thickness t at which on the average $\bar{A}=0.5$ of the total energy of a shower generated by a gamma quantum of energy $E_\gamma=(3375\pm125)$ MeV is absorbed in the medium fluctuates in a sample with $N_\gamma=15$ from ~4 to ~7.7 r.l. about a mean value of $t(\bar{A}=0.5)\cong5.5$ r.l. (shown by the dashed line in Fig. 42a). The inserts in these figures show the same cases of showers represented as the spread of the fraction A of energy deposition about the mean value $\bar{A}$ of this fraction determined for the given sample. For example, at the depth in liquid xenon at which on the average $\bar{A}=0.5$ of the total energy of a shower generated by a gamma quantum of energy $E_\gamma=(3375\pm125)$ MeV is absorbed in the medium, the fraction A varies from 0.25 to ~0.77 for a sample with $N_\gamma=15$ cases (dashed lines in the insert in Fig. 42a).

The question of the shape of the distributions of A and t for specified values of $\bar{A}$ and energy E_γ of the gamma quanta generating the showers is interesting. This question can to a large degree be resolved graphicaly, even for a small sample, by using probability paper (see, for example, Ref. 155, p. 91). In Figs. 43a and 43b we give two examples of the distribution of the fraction A for showers from primary gamma quanta with energy $E_\gamma=(3375\pm125)$ and (3125 ± 125) MeV, respectively. Ordered event samples at given values of $\bar{A}=0.1,0.2,...,0.9$ are plotted on probability paper following a normal distribution. The linear arrangement of points on this graph indicates that the sample distribution approximately obeys a normal law, although for $\bar{A}\gtrsim0.7$ the distributions, as expected, become asymmetric (because $A\leqslant1$) with kinks at $P_i=0.5$. Analogous distributions of the same events but in the shower development depth t suggest that the depths t at which fractions $A=0.1,0.2,...,0.9$ of the total shower energy are deposited

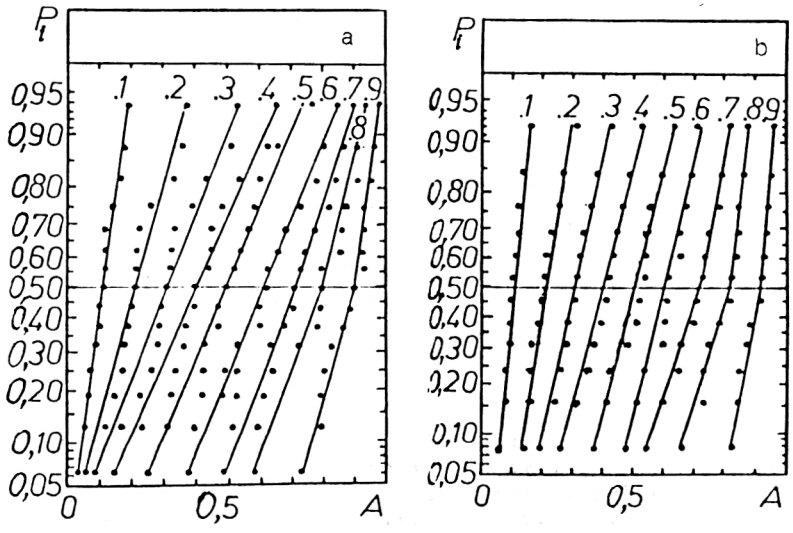

FIG. 43. Distribution of showers produced in liquid xenon by gamma quanta with energy (a) $E_\gamma=(3375\pm125)$ MeV and (b) $E_\gamma=(3125\pm125)$ MeV on probability paper for a normal distribution P_i of the fraction A of the total energy deposition of the shower. The average values $\bar{A}=0.1,0.2,...,0.9$ to which these distributions pertain are given in the upper part of the figure.[169]

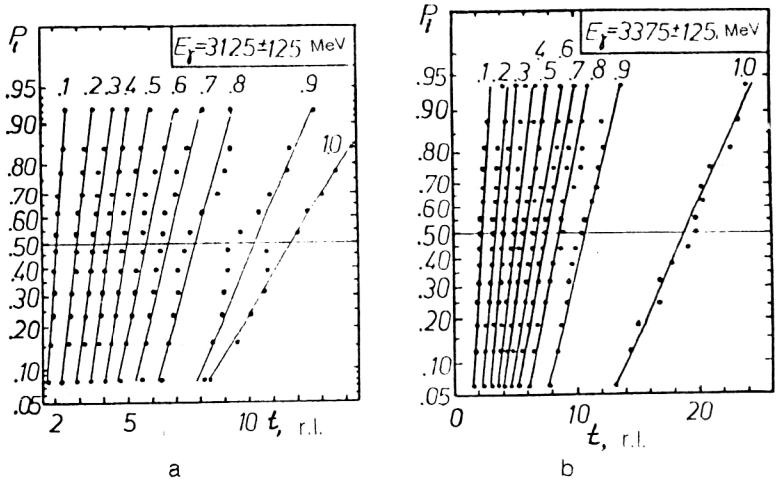

FIG. 44. The same as in Fig. 43 relative to the shower development depth t for (a) $E_\gamma=(3375\pm125)$ MeV and (b) $E_\gamma=(3125\pm125)$ MeV.

also approximately obey a normal distribution. The corresponding data are shown in Figs. 44a and 44b (Ref. 169).

Transverse fluctuations

Fluctuations in the transverse development of showers have been studied rather less than longitudinal ones. Meanwhile, it is they which determine, in particular, the spatial resolution of the gamma quanta recorded in hodoscopic gamma spectrometers (see, for example, Ref. 182) and which impose a natural limit on the transverse segmentation of electromagnetic calorimeters. Here we present the results of studies of the transverse fluctuations of the ionization energy losses in showers generated in liquid xenon by gamma quanta of energy $E_\gamma=100$–3500 MeV (Ref. 168), and also the fluctuations in the fraction of energy deposition about the geometrical axis of the shower.[170]

In Fig. 45 we show the distribution of the coefficient of the variation $\sigma_A^{(p)}/A$ of the energy-deposition fraction A in the transverse direction of the shower as a function of A for various values of the energy E_γ of the gamma quanta producing showers in liquid xenon. The fraction A was measured in the plane of the shower axis and summed over the shower depth. The coefficient $\sigma_A^{(p)}/A$ was normalized to its maximum value $(\sigma_A^{(p)}/A)_{\max}$, the energy dependence of which is shown in Fig. 46 and approximated by the function[172]

$$(\sigma_A^{(p)}/A)_{\max}=\alpha_p-\beta_p \ln E_\gamma, \tag{65}$$

where $\alpha_p=0.48\pm0.2$ and $\beta_p=(48\pm3)10^{-3}$. It should be noted that even though these data pertain to the plane of the shower axis, in going away from this axis they more and more accurately reflect the radial fluctuations of the ionization energy losses of shower electrons. As before, information on these fluctuations can be obtained by transforming, in the A dependence of the relative variation (Fig. 45), from the variable A to the relative distance $p/\bar{p}(E_\gamma)$ using the graphical relationship between these quantities (Fig. 39).

In the detection of high-energy gamma quanta the direction of the axis of the showers generated by them is reconstructed using the measured momenta from the counter cells of a transversely segmented hodoscope (see,

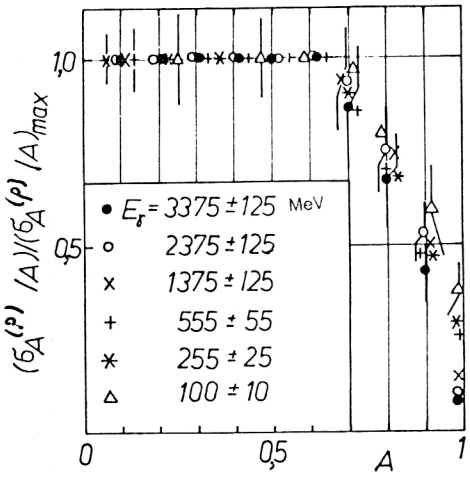

FIG. 45. The same as in Fig. 41 for the coefficient of variation of the fraction of the transverse energy deposition in showers. $(\sigma_A^{(p)}/A)_{\max}$ is the maximum value of this variation.[172]

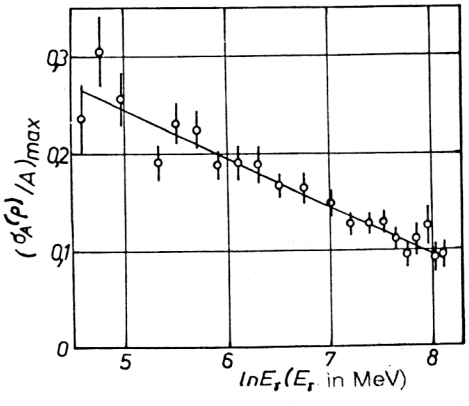

FIG. 46. Energy dependence of the maximum value of the variation coefficient $(\sigma_A^{(p)}/A)_{\max}$ of the transverse energy deposition in showers produced in liquid xenon by gamma quanta of energy E_γ (Ref. 172).

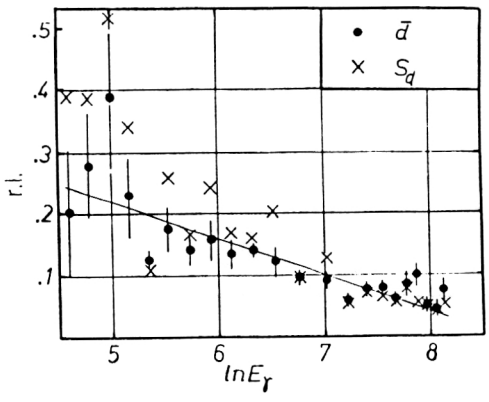

FIG. 47. Average distance $\bar{d}$ between the shower axis and the shower energy axis. S_d is the corresponding rms deviation. Showers are produced by gamma quanta of energy from 100 to 3500 MeV in liquid xenon.[170] The approximating function (66) is shown by the solid line (E_γ is in MeV).

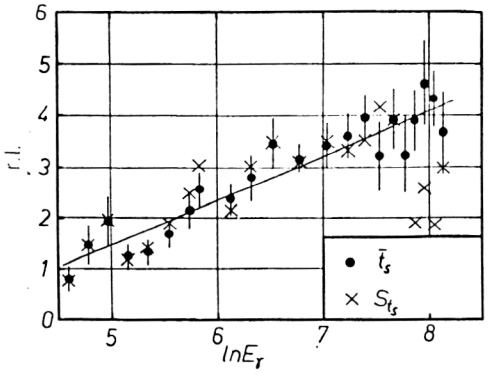

FIG. 48. Average value of the maximum shower depth $\bar{t}_s$ up to which the energy axis of the shower coincides with the geometrical axis of the shower. The approximating function (67) is shown by the solid line. S_{t_s} is the rms deviation of t_s from the average value (E_γ is in MeV).

for example, Ref. 78). Here it is assumed that the shower axis determined from the energy deposition (the energy axis of the shower) coincides with the geometrical axis, i.e., the line drawn through the points where the gamma quantum producing the shower appears and is converted. In Ref. 170 the XBC was used to study the fluctuations of the energy axis of the shower relative to its geometrical axis for energies E_γ of the primary gamma quanta producing showers in liquid xenon in the range from 100 to 3500 MeV.

In Fig. 47 we show the E_γ dependence of the average distance $\bar{d}$ between the shower axis and the shower energy axis, which lies in the plane of the photograph (which also contains the shower axis) and which separates the shower into two different parts (the energy axis of the shower is assumed to be parallel to the shower axis). There we also plot the values of the corresponding rms deviations S_d. The experimental data were approximated by the function[170]

$$\bar{d}=(0.52\pm0.03)-(59\pm4)10^{-3}\ln E_\gamma, \qquad (66)$$

which is also shown in this figure. Here $\bar{d}$ is in r.l. and E_γ is in MeV. As expected, $\bar{d}$ and S_d decrease with energy E_γ and for $E_\gamma \gtrsim 3$ GeV they are ~ 0.05 r.l.

Of practical interest, particularly in the case of segmentation for three-dimensional shower reconstruction,[183] is information on the depth t_s, measured from the start of the shower along its axis, to which the energy axis coincides with the shower axis. The distribution of the average symmetry depth $\bar{t}_s$, i.e., the average value of t_s, is shown in Fig. 48 together with the corresponding approximating function:[170]

$$\bar{t}_s=-(2.9\pm0.4)+(0.87\pm0.07)\ln E_\gamma, \qquad (67)$$

where $\bar{t}_s$ is in r.l. and E_γ is in MeV. In the same figure we plot the values of the rms deviation S_{t_s} of the symmetry depth t_s. The conclusion is that there are no noticeable correlations between the distance d and the depth t_s (the correlation coefficient for these quantities is less than 0.5). It should also be noted that the average distance between the energy and geometrical shower axes (the spatial distance) is roughly $\sqrt{2}\bar{d}$.

Fluctuations of the geometrical shape of the shower

It can be assumed that the coefficients of the variation of the average length $S_t/\bar{t}$ and the average width $S_p/\bar{p}$ of the shower development characterize the degree of diffusion of the volume of matter inside which the shower develops. In Fig. 49 we show the dependence of these variation coefficients on the energy E_γ of the gamma quanta producing showers in liquid xenon.[168] The corresponding approximating functions are plotted:

$$S_t/\bar{t}=0.61-5.77\cdot10^{-2}\ln E_\gamma, \qquad (68)$$

$$S_p/\bar{p}=3.38-3.33\cdot10^{-2}\ln E_\gamma. \qquad (69)$$

It is also interesting to compare the degree of diffuseness of the transverse and longitudinal boundaries of the shower. Such a comparison is made in Fig. 50 in the form of the energy dependence of the ratio of the rms deviations S_p/S_t. There we also show the energy dependence of the ratio $\bar{p}/\bar{t}$ of the average transverse and longitudinal shower dimensions. We see from these figures that the relative fluctuations of the transverse shower dimensions are about two times smaller than the longitudinal ones (i.e., $S_p/\bar{p}=(S_t/\bar{t})/2$; see Fig. 49) in the range of primary photon energies E considered, and that they decrease with increasing E_γ. The same trend is also observed in the ratio of the diffuseness of the transverse and longitudinal boundaries of the shower (Fig. 50). Figuratively speaking, as the energy of the gamma quanta increases the boundaries of the showers they produce become sharper and sharper, with the lateral profiles of the shower considerably sharper than the longitudinal ones. The showers themselves become more extended in the forward direction (for example, for $E_\gamma \cong 150$ MeV the ratio $\bar{p}/\bar{t}$ of the average transverse and longitudinal dimensions of the showers is ~ 0.6, while for $E_\gamma \cong 3000$ MeV it is ~ 0.2).

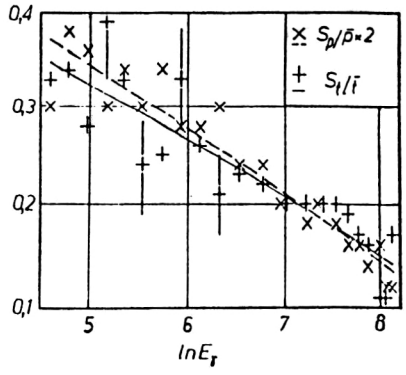

FIG. 49. Dependence of the coefficients of variation of the longitudinal $S_l/\bar{t}$ and transverse $S_p/\bar{p}$ shower development on the energy E_γ of the gamma quantum producing the showers in liquid xenon. The corresponding approximating functions (68) and (69) are shown by the lines (E_γ is in MeV).[149]

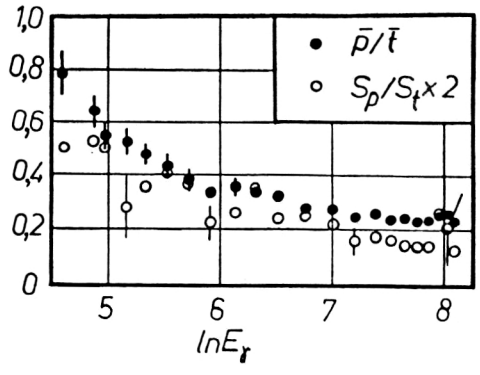

FIG. 50. Ratio of the rms scatter of the transverse S_p and longitudinal S_l dimensions of showers produced in liquid xenon by gamma quanta of energy E_γ (Ref. 167). $\bar{p}/\bar{t}$ is the ratio of the average values of the transverse ($\bar{p}$) and longitudinal ($\bar{t}$) shower development lengths (E_γ is in MeV).

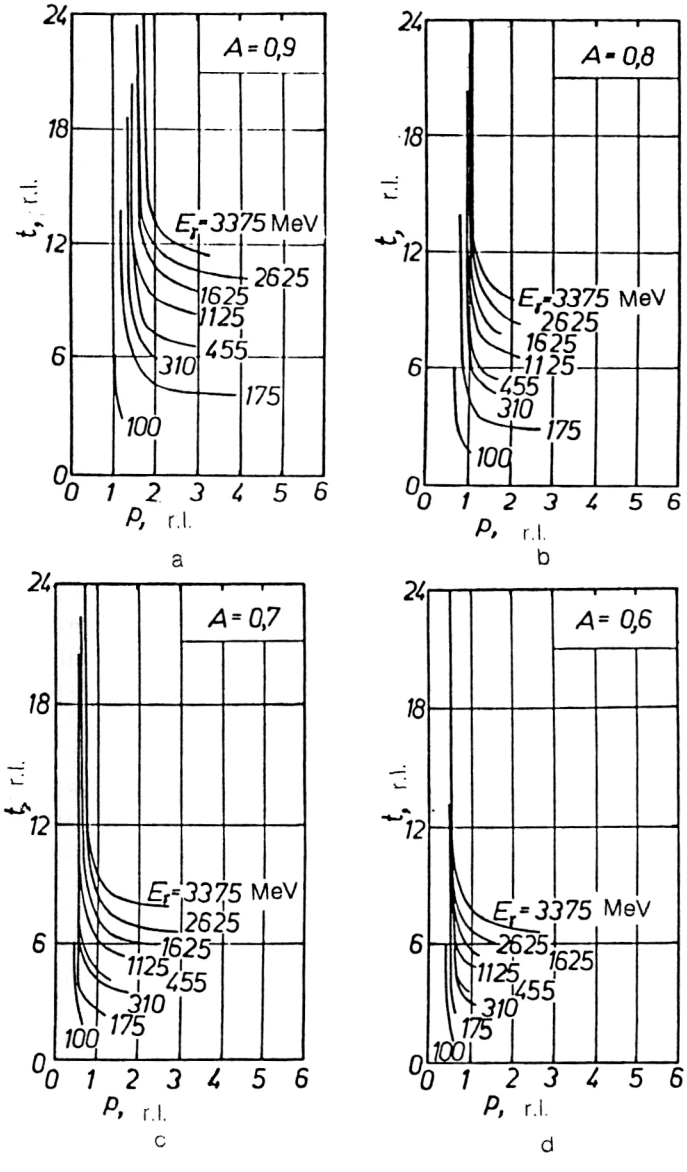

FIG. 51. Averaged correlation curves in the plane of the shower axis: on the average, a fraction (a) $A=0.9$, (b) 0.8, (c) 0.7, and (d) 0.6 of the total energy of showers produced by gamma quanta of energy E_γ is released inside a volume of liquid xenon of thickness t and width $2p$ (Ref. 171).

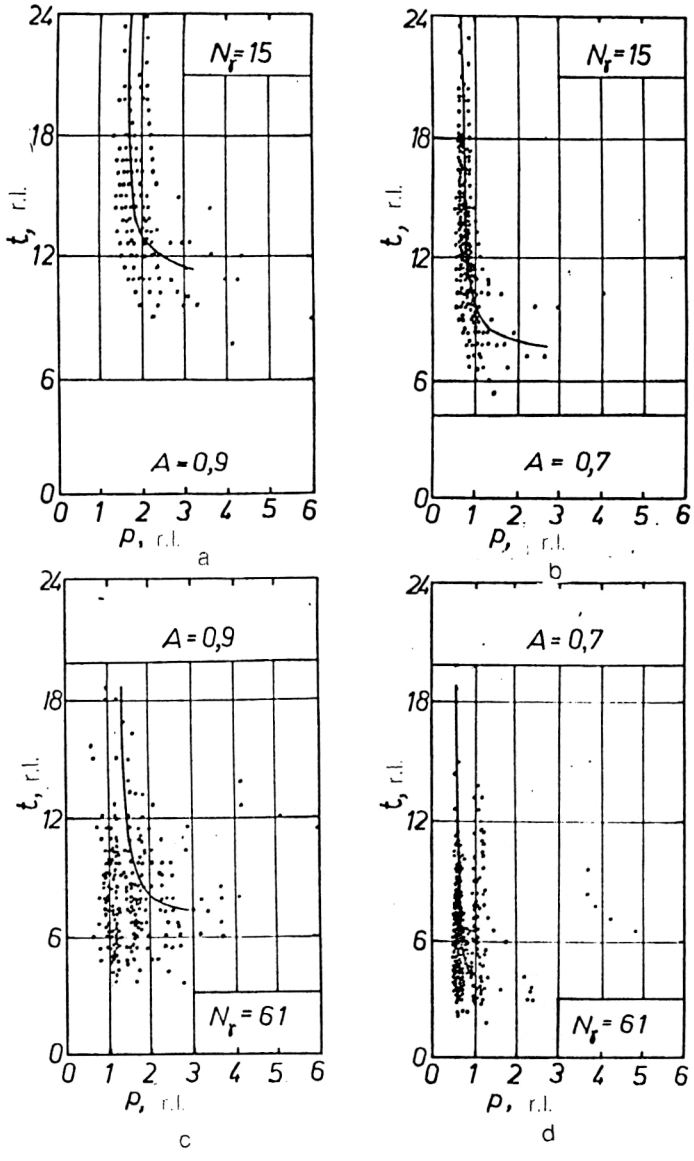

FIG. 52. Graph of the distribution of showers produced in liquid xenon by gamma quanta of energy $E_\gamma=(3375\pm125)$ MeV [*a* and *b*] and $E_\gamma=(375\pm35)$ MeV [*c* and *d*]; t and p are the thickness and width of the layer of liquid xenon inside which the fraction $A=0.9$ and $A=0.7$ (shown on the figures) of the total shower energy is released. N_γ is the size of the sample of analyzed shower events. The curve shows the result of the averaging. The data are from Ref. 171.

Correlations

This important topic has become a subject of experimental study only relatively recently. Two questions of practical interest have been studied, and the experimental data was obtained using XBCs. The authors of Ref. 171 studied the correlations (in the plane of the shower axis) between the length t and width p of development of showers produced in liquid xenon by gamma quanta of energy $E_\gamma=100$–3500 MeV. The correlations between t and p were studied with the condition that exactly a fraction $A=0.9,0.8,0.7$, and 0.6 of the total shower energy was detected. The corresponding experimental data are shown in Fig. 51 for the eight indicated values of the energy E_γ. A point (t,p) on a curve at a given energy E_γ means that on the average a fraction A (shown on the figure) of this energy is released in a volume of liquid xenon of thickness t and width $2p$. In other words, the values of t and p at a given energy E_γ and fixed A are correlated on the average, which is seen from these figures. However, owing to the transverse and longitudinal fluctuations each such dependence is statistical in nature and in fact represents a graph of the distribution of points (t,p) scattered near the averaged dependence, which is shown as a curve. An example of the graphs obtained in Ref. 171 of the distribution of points (t,p) is shown in Fig. 52 for the two values $E_\gamma=(3375\pm125)$ and (375 ± 35) MeV and the two values $A=0.9$ and 0.7. There we also give the number N_γ of cases in each sample.

It follows from these data in particular that owing to the significant fluctuations of the spatial dimensions of showers it is insufficient to measure the energy deposited inside a volume of thickness t and width $2p$ in order to somehow judge the energy of the primary gamma quantum if the spatial structure of this energy deposition is unknown.

The authors of Ref. 169 studied the correlations in the longitudinal distribution of the ionization energy losses of individual showers generated in liquid xenon by gamma quanta of energy $E_\gamma=100$–3500 MeV. We recall that in the graph of $(\bar{A},t)$ (Figs. 42a and 42b) the points farthest from

TABLE XII. Values of the correlation coefficient r_{ij} given by Eq. (70). $E_\gamma=(3375\pm125)$ MeV.

i \ j	3	4	5	6	7	8	9	10
2	0,52	0,64	0,48	0,42	0,07	0,38	0,02	0,19
3		0,79	0,49	0,42	0,18	0,26	0,41	0,48
4			0,76	0,62	0,33	0,25	0,34	0,27
5				0,90	0,43	0,02	0,13	0,11
6					0,45	0,77	0,26	0,08
7						0,24	0,24	0,22
8							0,14	0,48
9								0,14

the solid line are connected by straight-line segments such that each broken line is an individual case of a shower or, in other words, a realization of the random function of the accumulated probability of the longitudinal ionization energy losses (henceforth referred to as the random function). It may be noted that with increasing energy E_γ the random shower functions become smoother on the average. This suggests that the observed form of the distribution of the energy deposited in a shower up to a certain development depth can give information on how much energy is deposited at large depths and, therefore, on the total energy of the shower. In other words, it can give information on how strongly the individual segments of the random shower function are correlated with each other during the course of the shower development. To obtain a quantitative estimate of these correlations we use the standard definition of the correlation coefficient

$$r_{ij}=\mathrm{cov}(X_i,X_j)/[\sigma(X_i)\sigma(X_j)], \tag{70}$$

where $X_i=\Delta\bar{A}/\Delta t_i$ is the slope of the random function at the depth t_i of the liquid xenon at which on the average $i/10$ of the total shower energy is absorbed ($i=2,3,..,10$), and the thickness of the layer $\Delta t_i=t_i-t_{i-1}$ is chosen such that on the average a fraction $\Delta\bar{A}=0.1$ of this energy is absorbed in it ($j>i$). The numerical values of the coefficient r_{ij} for two of the six values of the energy E_γ analyzed in Ref. 169, $E_\gamma=(3375\pm125)$ and (555 ± 55) MeV are given in Tables XII and XIII.

Although the small statistics of the analyzed events does not allow definitive conclusions to be made, it can still be noted that in the range $E_\gamma=100$–3375 MeV of energies of gamma quanta producing showers in liquid xenon, only short-range correlations of the longitudinal energy release in the vicinity of the shower maximum (i.e., for $i=4$–7) are observed.[169]

6. CONCLUSION

In recent years significant progress has been made in the study of the main characteristics of electron–photon showers produced in heavy amorphous media by gamma quanta and electrons at accelerator energies. The wide variety of available experimental data can, in principle, be described within the framework of modeling showers by the Monte Carlo method, and the corresponding computer programs are constantly being improved by the more accurate inclusion of the elementary physical processes and, of exceptional importance, the use of various algorithms for faster and faster modeling.

The results of measurements of the longitudinal shower profile can be represented as a universal distribution, at least for sufficiently high energies of the gamma quanta (and electrons) generating the showers ($\gtrsim$ 500 MeV) if the average shower development length is taken as the length scaling parameter. A universal cascade curve can also be constructed using the location of the shower maximum or its median as this parameter (see, for example, Ref. 117). This representation of the longitudinal shower development averaged over fluctuations is apparently valid to energies of several TeV, since at higher en-

TABLE XIII. The same as in Table XII for $E_\gamma=(555\pm55)$ MeV.

i \ j	3	4	5	6	7	8	9	10
2	0,64	0,13	0,08	0,14	0,11	0,10	0,08	0,04
3		0,70	0,26	0,04	0,02	0,08	0,11	0,05
4			0,68	0,20	0,15	0,08	0,01	0,03
5				0,55	0,30	0,23	0,06	0,02
6					0,68	0,44	0,14	0,14
7						0,68	0,25	0,22
8							0,33	0,01
9								0,03

ergies the effective cross sections of electromagnetic and weak interactions become comparable, so that the shower is enriched by hadrons and neutrinos. This in turn leads to a significant increase of the longitudinal dimensions of the shower. Figuratively speaking, a shower begins to lengthen, first at the start of its development and, as the energy grows, gradually over the entire depth it occupies. In addition, at energies of $\sim 10^{13}$ eV and above the LPM effect becomes more and more important. It also produces a gradual lengthening of the longitudinal dimensions, but only of the electromagnetic component of the shower. However, deviation from the "standard" form (51) of a shower produced by gamma quanta begins already at an energy of ~ 100 GeV owing to the Chudakov effect. This deviation is not difficult to take into account by shifting the corresponding point where the shower starts along the shower axis to the point at which the mutual screening of the electron and positron of the pair is unimportant. This procedure has practically no effect on the energy balance of the shower. It increases only the longitudinal fluctuations, which are equivalent to fluctuations of the conversion length of the primary gamma quantum. It should also be noted that a significant compression of the longitudinal dimensions of the electromagnetic component of a shower can be obtained using the effect of the coherent interaction of photons and electrons incident on a single crystal at sufficiently small angles relative to one of its crystal axes. However, here, owing to the simultaneous channeling of the hadrons, their mean free path grows considerably. Therefore, a single crystal acts as a separator of the electromagnetic and hadronic parts of a shower generated by a particle of sufficiently high energy.

Another important shower characteristic on which rather diverse experimental data have been obtained is the transverse profile. As shown by the present author, again in this case it is possible to obtain a universal description of the radial distribution of the ionization energy losses using, as before, the average width of the shower as the scaling parameter. The longitudinal and transverse fluctuations in showers can also be represented in universal form.

Finally, we note that the correlations between various characteristics of electron–photon showers have been studied very little. This is a very complicated technical problem from the experimental point of view. However, such results are needed for studying particle multiple production processes at high and superhigh energies, which will be done at accelerators of future generations using finely segmented electromagnetic calorimeters.

[1)] Various synonyms are used in the literature to refer to this process: electromagnetic cascade, cascade shower, electron–photon cascade, and so on.

[2)] Since in most shower detectors it is not possible to distinguish electrons from positrons, as a rule the term electrons refers to the sum of electrons and positrons.

[3)] References to other studies on experimental shower investigations can be found in the publications cited here.

[4)] This quantity is somewhat larger than the analogous estimates given in the literature for liquid xenon (see, for example, Ref. 92), since the XBC contains an addition of 0.5% ethylene by weight[90] or 1% propane and 0.7% ethylene by volume[89] for extinguishing the scintillations and obtaining reliable sensitivity to ionizing radiation. Henceforth we shall take the radiation length in the XBC to be 4 cm. The radiation length is defined in Sec. 2.

[5)] Various synonyms can be encountered in the literature: radiation length, radiation unit, shower unit, t unit, cascade unit.

[6)] The other possible interpretation of this event is less probable.

[7)] In the case of a simplified modeling scheme it is appropriate to consider different variants of the model in order to be able to estimate the degree to which the final result can depend on the assumptions which are made.

[1] B. Rossi, Phys. Z. **33**, 304 (1932).
[2] B. Rossi, *High-Energy Particles* (Prentice-Hall, New York, 1952) [Russ. transl., Gostekhizdat, Moscow, 1955].
[3] W. Heitler, *The Quantum Theory of Radiation*, 3rd. ed. (Clarendon Press, Oxford, 1954) [Russ. transl., IL, Moscow, 1956].
[4] P. M. S. Blackett and G. P. S. Occhialini, Proc. Roy. Soc. London Ser. A **139**, 600 (1933); P. M. S. Blackett, G. P. S. Occhialini, and J. Chadwick, Proc. Roy. Soc. London Ser. A **144**, 235 (1934).
[5] H. J. Bhabha and W. Heitler, Proc. Roy. Soc. London Ser. A **159**, 432 (1937).
[6] J. F. Carlson and J. R. Oppenheimer, Phys. Rev. **51**, 220 (1937).
[7] L. Landau and G. Rumer, Proc. Roy. Soc. London Ser. A **166**, 213 (1988).
[8] S. Z. Belen'kiĭ, *Shower Processes in Cosmic Rays* [in Russian] (OGIZ, Moscow, 1948).
[9] J. Nichimura, Handbuch der Physik, Vol. XLVI/2, p. 1 (1967) (Springer-Verlag, Berlin).
[10] I. P. Ivanenko, *Electromagnetic Cascade Processes* [in Russian] (Moscow State University Press, Moscow, 1972).
[11] B. Rossi and K. Greisen, Rev. Mod. Phys. **13**, 240 (1941).
[12] A. Ramakrishnan, *Elementary Particles and Cosmic Rays* (Pergamon Press, New York, 1962) [Russ. transl., Mir, Moscow, 1965].
[13] I. P. Ivanenko, V. M. Maksimenko, and V. V. Sizov, Preprint 296, Lebedev Institute, Moscow (1986) [in Russian].
[14] A. L. Zachary, Phys. Rev. D **37**, 112 (1988).
[15] H. Euler and H. Wergeland, Astrophys. Norv. **3**, 163 (1940).
[16] G. Molière, in *Kosmische Strahlung*, W. Heisenberg (Springer, Berlin, 1953).
[17] J. Roberg and W. Nordheim, Phys. Rev. **75**, 444 (1949).
[18] L. Eyges and S. Fernbach, Phys. Rev. **82**, 23 (1951).
[19] H. S. Green and H. Messel, Phys. Rev. **88**, 331 (1952).
[20] I. P. Ivanenko and T. M. Roganova, *Cascade Showers Induced by Particles of Superhigh Energy* [in Russian] (Nauka, Moscow, 1983).
[21] R. R. Wilson, Phys. Rev. **86**, 261 (1952).
[22] M. Ya. Borkovskiĭ, Preprint 462, Leningrad Nuclear Physics Institute, Gatchina (1979) [in Russian].
[23] B. E. Shtern, Preprint P-0081, Nuclear Physics Institute Moscow (1978) [in Russian].
[24] T. Stanev and Ch. Vankov, Bulg. J. Phys. **5**, 433 (1978).
[25] I. A. Amatuni, "ELSSI. A Universal Program for Modeling Electromagnetic High-Energy Showers by the Monte Carlo Method," Report EFI-760/75/-84, Erevan (1984) [in Russian].
[26] W. R. Nelson, H. Hirayama, and W. O. Rogers, SLAC Report 265, SLAC, Palo Alto (1985).
[27] R. Brun *et al.*, "GEANT User's Guide," Report DD/EE/84-1, CERN, Geneva (1986).
[28] W. R. Nelson and Y. Namito, SLAC-PUB-5193, SLAC, Palo Alto (1990).
[29] E. Longo and J. Sestili, Nucl. Instrum. Methods **128**, 283 (1975).
[30] A. De Angelis, Nucl. Instrum. Methods A **271**, 455 (1988).
[31] G. Gringhammer, M. Rudowicz, and S. Peters, Nucl. Instrum. Methods A **290**, 469 (1990).
[32] S. L. Linn, Nucl. Instrum. Methods A **288**, 598 (1990).
[33] S. L. Linn and E. M. Wang, Preprint FSU-SCRI-89C-88 (1989).
[34] N. Fujimaki and A. Misaki, ICR-Report-165-88-14 (1988).
[35] M. Okamoto and T. Shibata, Nucl. Instrum. Methods A **257**, 155 (1987).
[36] J. Del Peso and E. Ros, Nucl. Instrum. Methods A **306**, 485 (1991).
[37] S. A. Sadovskiĭ, Preprint IHEP 85-34, IHEP, Serpukhov (1985) [in Russian].
[38] B. Słowiński, JINR Communication E1-89-658, JINR, Dubna (1989).
[39] A. Misaki, ICR-Report-183-88-29 (1988).
[40] I. P. Ivanenko, A. A. Kirillov, and Yu. G. Lyutov, Preprints No. 165 and 166, Lebedev Institute, Moscow (1986) [in Russian].

[41] P. K. Job, G. Sterzenbach, and D. Filges, Nucl. Instrum. Methods A **271**, 442 (1988).
[42] N. Takahashi, Nucl. Instrum. Methods A **270**, 347 (1988).
[43] D. Acosta, S. Buontempo, L. Caloba *et al.*, Nucl. Instrum. Methods A **316**, 184 (1992).
[44] M. Anghinolfi, M. Castoldi, and P. Corvisiero, Nucl. Instrum. Methods A **317**, 531 (1992).
[45] P. S. Takhar, Nuovo Cimento A **89**, 76 (1985).
[46] O. A. Zaĭmidoroga, Yu. D. Prokoshkin, and V. M. Tsupko-Sitnikov, Zh. Eksp. Teor. Fiz. **51**, 749 (1966) [Sov. Phys. JETP **24**, 498 (1967)]; Zh. Eksp. Teor. Fiz. **52**, 79 (1967) [Sov. Phys. JETP **25**, 51 (1967)].
[47] E. Beclin and J. Earl, Phys. Rev. **136**, B237 (1964).
[48] H. Thom, Phys. Rev. **136**, B447 (1964).
[49] A. N. Gapotchenko, B. B. Govorkov, S. P. Denisov *et al.*, Prib. Tekh. Eksp. No. 5, 60 (1966) [Instrum. Exp. Tech.].
[50] A. M. Zaĭtsev, I. A. Radkevich, and Yu. F. Tomashchuk, Prib. Tekh. Eksp. No. 4, 852 (1969) [Instrum. Exp. Tech.].
[51] D. I. Sober, R. P. Haddock, B. M. K. Nefkens, and B. L. Schrock, Nucl. Instrum. Methods **109**, 29 (1973).
[52] J. W. Cronin, E. Engels, M. Pyka *et al.*, Rev. Sci. Instrum. **33**, 946 (1962).
[53] R. Kajikawa, J. Phys. Soc. Jpn. **18**, 1365 (1963).
[54] Y. Murata, J. Phys. Soc. Jpn. **20**, 209 (1965).
[55] H. Lengler, W. Tejessy, and M. Deutschman, Z. Phys. **175**, 283 (1963); Nuovo Cimento **28**, 1501 (1963).
[56] B. Słowiński, Z. Strugal'skiĭ, and B. Yanovskaya, Yad. Fiz. **9**, 120 (1969) [Sov. J. Nucl. Phys. **9**, 73 (1969)].
[57] B. Słowiński, Z. Strugal'skiĭ, and V. Hubert, Yad. Fiz. **16**, 734 (1972) [Sov. J. Nucl. Phys. **16**, 410 (1972)].
[58] D. J. Drickey, J. R. Kilner, and D. Benaksas, Phys. Rev. **171**, 310 (1968).
[59] G. S. Bitsadze, Yu. A. Budagov, V. V. Glagolev *et al.*, Nucl. Instrum. Methods A **251**, 61 (1968).
[60] C. A. Hensch and C. Y. Prescott, Phys. Rev. **135**, B772 (1964).
[61] H. Hirajama, S. Ban, S. Miura, Preprint 86-97, KEK, Japan (1987).
[62] G. S. Bitsadze, V. M. Maniev, I. A. Minashvili *et al.*, Preprint E1-86-87, JINR, Dubna (1986).
[63] Yu. D. Prokoshkin and Tian Siao-Wei, Zh. Eksp. Teor. Fiz. **36**, 10 (1959) [Sov. Phys. JETP **9**, 6 (1959)].
[64] O. A. Zaĭmidoroga, Yu. D. Prokoshkin, V. Kut'in *et al.*, Zh. Eksp. Teor. Fiz. **55**, 2180 (1968) [Sov. Phys. JETP **28**, 1156 (1969)].
[65] A. S. Belousov, E. I. Malinovskiĭ, S. V. Rusakov *et al.*, Yad. Fiz. **17**, 1028 (1973) [Sov. J. Nucl. Phys. **17**, 537 (1973)].
[66] W. Blocker, R. Kenney, and W. Panofsky, Phys. Rev. **79**, 419 (1950).
[67] C. Gramel, Phys. Rev. **161**, 310 (1967).
[68] W. Nelson, T. Jenkins, R. McCall *et al.*, Phys. Rev. **149**, 201 (1966).
[69] N. Takahashi, Nucl. Instrum. Methods A **270**, 347 (1988).
[70] K.-P. Beuermann and G. Wibberenz, Z. Phys. **206**, 247 (1967).
[71] R. Jakeways and J. R. Calder, Nucl. Instrum. Methods **84**, 79 (1970).
[72] D. Muller, Phys. Rev. D **5**, 2677 (1972).
[73] G. Bathow, E. Freytag, M. Kobberling *et al.*, Nucl. Phys. B **20**, 592 (1970).
[74] T. Yuda, Nucl. Instrum. Methods **73**, 301 (1969).
[75] K. Kleinknecht, *Detectors for Particle Radiation* (Cambridge Univ. Press, Cambridge, 1986).
[76] N. V. Rabin, Prib. Tekh. Eksp. No. 1, 12 (1992) [Instrum. Exp. Tech.].
[77] G. Barbiellini, G. Cecchet, J. Y. Hemery *et al.*, Nucl. Instrum. Methods A **236**, 316 (1985).
[78] G. A. Akopdjanov, A. V. Inyakin, V. A. Kachanov *et al.*, Nucl. Instrum. Methods **140**, 441 (1977).
[79] G. Barbiellini, G. Cecchet, J. Y. Hemery *et al.*, Nucl. Instrum. Methods A **240**, 289 (1985).
[80] R. Rameika, B. Cox, M. Jenkins *et al.*, IEEE Trans. Nucl. Sci. *NS*—31, 60 (1984).
[81] G. Barbiellini, G. Cecchet, J. Y. Hemery *et al.*, Nucl. Instrum. Methods A **235**, 55 (1985).
[82] F. Bianchi, E. Castelli, P. Checchia *et al.*, Nucl. Instrum. Methods A **279**, 473 (1989).
[83] F. Lemeilleur, F. Lamarche, C. Leroy *et al.*, Preprint CERN-EP/89-27, CERN, Geneva (1989).
[84] G. Ferri, F. Groppi, F. Lemeilleur *et al.*, Nucl. Instrum. Methods A **273**, 123 (1988).
[85] E. Hughes, Preprint SLAC-PUB 5404, SLAC, Palo Alto (1990).
[86] W. Badgett, R. Ball, Y. Cha *et al.*, Nucl. Instrum. Methods A **307**, 231 (1991).
[87] D. Acosta, S. Buontempo, L. Caloba *et al.*, Nucl. Instrum. Methods A **308**, 481 (1991).
[88] D. Acosta, S. Buontempo, L. Caloba *et al.*, Nucl. Instrum. Methods A **316**, 184 (1992).
[89] E. V. Kuznetsov, A. N. Rozanov, Yu. V. Bardyukov *et al.*, Prib. Tekh. Eksp. No. 2, 56 (1970) [Instrum. Exp. Tech.].
[90] T. Kanarek, E. I. Maltsev, T. Nagy *et al.*, in *Proc. of the Intern. Conf. on High Energy Accelerators and Instrumentation*, CERN, Geneva (1958), p. 508.
[91] B. Nichiporuk, B. Słowiński, and Z. Strugal'skiĭ, Preprint R-2808, JINR, Dubna (1966) [in Russian].
[92] Particle Data Group, Rev. Mod. Phys. **56**, S53 (1984).
[93] A. Baranov, V. Baskakov, G. Bondarenko *et al.*, Nucl. Instrum. Methods A **294**, 439 (1990).
[94] M. Chen, C. Dionisi, Yu. Galaktionov *et al.*, Nucl. Instrum. Methods A **267**, 43 (1988).
[95] A. Braem, A. Gonidec, D. Schinzel *et al.*, Nucl. Instrum. Methods A **320**, 228 (1992).
[96] A. I. Akhiezer and V. Yu. Berestetskiĭ, *Quantum Electrodynamics* (Wiley, New York, 1965) [Russ. original, Nauka, Moscow, 1981].
[97] H. Messel and D. F. Crawford, *Electron–Photon Shower Distribution Function* (Pergamon Press, Oxford, 1970).
[98] J. A. Wheeler and W. A. Lamb, Phys. Rev. **55**, 858 (1939).
[99] L. Landau and I. Pomeranchuk, Dok. Akad. Nauk SSSR **92**, 735 (1953).
[100] A. B. Migdal, Phys. Rev. **103**, 1811 (1956).
[101] E. Kanichi, A. Adachi, N. Takahashi, and A. Misaki, J. Phys. G **17**, 719 (1991).
[102] C. Moller, Ann. Phys. (Leipzig) **14**, 531 (1932).
[103] H. J. Bhabha, Proc. Roy. Soc. London Ser. A **154**, 195 (1936).
[104] H. A. Bethe, Ann. Phys. (Leipzig) **5**, 325 (1930).
[105] H. A. Bethe, Z. Phys. **76**, 293 (1932).
[106] F. Bloch, Z. Phys. **81**, 363 (1933).
[107] R. M. Sternheimer, Phys. Rev. **88**, 851 (1952).
[108] F. Rohrlich and B. C. Carlson, Phys. Rev. **93**, 38 (1954).
[109] T. W. Armstrong and R. G. Alsmiller, Jr., Nucl. Instrum. Methods **82**, 289 (1970).
[110] D. M. Ritson, in *Proc. of the Summer Institute on Particle Physics*, SLAC Report No. 239 (1981).
[111] "Stopping Powers for Electrons and Positrons," ICRU Report 37, Intern. Commission on Radiation Units and Measurements, Washington, D.C. (1984).
[112] S. Hayakawa, *Cosmic Ray Physics: Nuclear and Astrophysical Aspects* (Wiley, New York, 1969) [Russian transl., Mir, Moscow, 1973].
[113] R. M. Sternheimer, Phys. Rev. **145**, 247 (1966).
[114] L. D. Landau and E. M. Lifshitz, *Quantum Mechanics*, 3rd ed. (Pergamon Press, Oxford, 1977) [Russian original, Gos. izd-vo fiz.-mat. lit., Moscow, 1963].
[115] L. Pages, E. Bertel, H. Joffre, and L. Sklavenitis, Report CEA-R-3942, Saclay (1970).
[116] E. Fermi, Phys. Rev. **57**, 475 (1940).
[117] A. N. Kalinovskiĭ, N. V. Mokhov, and Yu. P. Nikitin, *The Passage of High-Energy Particles Through Matter* [in Russian] (Energoatomizdat, Moscow, 1985).
[118] L. D. Landau, *Collected Works* [in Russian], Vol. 1 (Nauka, Moscow, 1969).
[119] R. M. Sternheimer, Phys. Rev. **88**, 851 (1952).
[120] O. Blunck and S. Leisegang, Z. Phys. **128**, 500 (1950).
[121] P. V. Vavilov, Zh. Eksp. Teor. Fiz. **32**, 920 (1957) [Sov. Phys. JETP **5**, 749 (1957)].
[122] V. K. Ermilova and V. A. Chechin, Preprint No. 10, Lebedev Institute, Moscow (1976) [in Russian].
[123] W. W. M. Allison and J. H. Cobb, Ann. Rev. Nucl. Sci. **30**, 253 (1980).
[124] K. O'Brien, in *Computer Techniques in Radiation Transport and Dosimetry*, edited by W. R. Nelson and M. Jenkins (Plenum, New York, 1978), p. 141.
[125] G. Molière, Z. Naturforsch Teil A **3**, 78 (1948).
[126] H. A. Bethe, Phys. Rev. **89**, 1256 (1953).
[127] L. N. Cooper and J. Rainwater, Phys. Rev. **97**, 492 (1955).
[128] W. T. Scott, Rev. Mod. Phys. **35**, 231 (1963).
[129] O. Klein and Y. Nishina, Z. Phys. **25**, 853 (1929).

[130] R. H. Pratt, Phys. Rev. **10**, 1717 (1961).
[131] J. V. Jelley, *Čerenkov Radiation and Its Applications* (Pergamon Press, Oxford, 1958) [Russ. transl., IL, Moscow, 1960].
[132] D. H. Perkins, *Introduction to High Energy Physics* (Addison-Wesley, Reading, Mass., 1982).
[133] R. R. Roy and R. D. Reed, *Interactions of Photons and Leptons With Matter* (Academic Press, New York, 1968).
[134] W. W. M. Allison and P. R. S. Wright, Preprint OUNP 35/83, Oxford University (1983).
[135] A. E. Chudakov, Izv. Akad. Nauk SSSR, Ser. Fiz. **19**, 650 (1955) [Bull. Acad. Sci. USSR, Phys. Ser.].
[136] G. Yekutieli, Nuovo Cimento **5**, 1381 (1957).
[137] U. Amaldi, Physica Scripta **23**, 409 (1981).
[138] O. I. Dovzhenko and A. A. Pomanskiı, Zh. Eksp. Teor. Fiz. **45**, 268 (1963) [Sov. Phys. JETP **18**, 187 (1964)].
[139] I. Adamchevskiĭ, K. Kozlovskiĭ, Ya. Piatkovska *et al.*, JINR Report 13-6676, JINR, Dubna (1972) [in Russian].
[140] Z. Strugalski, JINR Report No. 796, JINR, Dubna (1961).
[141] L. P. Konovalova, L. S. Okhrimenko, and Z. Strugal'skiĭ, Prib. Tekh. Eksp. No. 6, 26 (1961) [Instrum. Exp. Tech.].
[142] O. Czyżewski, J. Danysz, and Z. Strugalski, Acta Phys. Pol. **24**, 509 (1963).
[143] I. A. Ivanovskaya, T. Kanarek, L. S. Okhrimenko *et al.*, Prib. Tekh. Eksp. No. 2, 39 (1968) [Instrum. Exp. Tech.].
[144] V. V. Barmin, V. G. Barylov, V. M. Golubchikov *et al.*, Preprint 938, ITEP, Moscow (1972) [in Russian].
[145] M. Ya. Borkovskiĭ and S. P. Kruglov, Preprint No. 184, Leningrad Nuclear Physics Institute, Gatchina (1975) [in Russian].
[146] B. Nichiporuk and Z. Strugal'skiı, Zh. Eksp. Teor. Fiz. **45**, 13 (1963) [Sov. Phys. JETP **18**, 10 (1964)].
[147] A. A. Tyapkin, Nucl. Instrum. Methods **85**, 277 (1970).
[148] B. Słowiński, B. Srednyava, and Z. Strugal'skiĭ, Preprint R1-9198, JINR, Dubna (1975) [in Russian].
[149] B. Słowiński, JINR Communication E1-91-230, Dubna (1991).
[150] V. V. Uchaikin and A. A. Lagutkin, Izv. Akad. Nauk SSSR, Ser. Fiz. **39**, 1255 (1975) [Bull. Acad. Sci. USSR, Phys. Ser.].
[151] V. V. Vetoshkin and V. V. Uchaikin, Preprint ITEP 87-12, Alma-Ata (1987) [in Russian].
[152] B. Słowiński, in *Proc. of the Intern. Conf. on Problems in Mathematical Modeling in Nuclear Physics Research*, Dubna, 1980, Reports JINR D10, 11-81-622, JINR, Dubna (1981), p. 178 [in Russian].
[153] S. M. Ermakov and G. A. Mikhailov, *Statistical Modeling* [in Russian] (Nauka, Moscow, 1982).
[154] S. M. Ermakov, *The Monte Carlo Method and Related Problems* [in Russian] (Nauka, Moscow, 1971).
[155] D. J. Hudson, "Lectures on Elementary Statistics and Probability," CERN Report (unpublished), Geneva (1964) [Russian transl., Mir, Moscow, 1967].
[156] J. W. Butler, in *Symp. on Monte Carlo Methods*, edited by H. A. Meyer (Wiley, New York, 1966).
[157] B. Słowiński, Preprint R13-88-239, JINR, Dubna (1988) [in Russian].
[158] B. Słowiński, D. Chizhevska, G. Endzheets, and R. Wisnewski, Preprint R1-86-809, JINR, Dubna (1986) [in Russian].
[159] Z. Ogrzeval'skiĭ and Z. Strugal'skiĭ, Preprint R1-4077, JINR, Dubna (1968) [in Russian].
[160] Z. Ogrzeval'skiĭ and Z. Strugal'skiĭ, Preprint R1-4562, JINR, Dubna (1969) [in Russian].
[161] A. Gładki and Z. Jabłoński, Zeszyty Naukowe Uniwersytetu Łodzkiego, Ser. II, No. 12, 99 (1977).
[162] B. Słowiński, JINR Communication E1-89-676, JINR, Dubna (1989).
[163] L. S. Okhrimenko, B. Słowiński, Z. Strugal'skiĭ *et al.*, Preprint R1-11980, JINR, Dubna (1978) [in Russian].
[164] L. S. Okhrimenko, B. Słowiński, and Z. Strugal'skiĭ, Yad. Fiz. **22**, 110 (1975) [Sov. J. Nucl. Phys. **22**, 218 (1975)].
[165] B. Słowiński and V. Chaĭ, Preprint R1-80-341, JINR, Dubna (1980) [in Russian]; Izv. Akad. Nauk SSSR, Ser. Fiz. **45**, 1230 (1981) [Bull. Acad. Sci. USSR, Phys. Ser.].
[166] B. Słowiński, D. Chizhevska, G. Endzheets, and R. Wisnewski, Preprint R1-86-810, JINR, Dubna (1986) [in Russian].
[167] B. Słowiński, D. Chizhevska, G. Endzheets, and R. Wisnewski, Preprint R1-86-811, JINR, Dubna (1986) [in Russian].
[168] B. Słowiński, JINR Communication E1-90-274, JINR, Dubna (1990).
[169] B. Słowiński, JINR Rapid Communications No. 3[49]-91, 5 (1991).
[170] B. Słowiński, JINR Rapid Communications No. 1[52]-92, 17 (1992).
[171] B. Słowiński, JINR Communication E1-90-273, JINR, Dubna (1990).
[172] B. Słowiński, JINR Communication E1-90-277, JINR, Dubna (1990).
[173] B. Słowiński, JINR Communication E1-89-789, JINR, Dubna (1989).
[174] W. Czaj, Rozprawa doktorska, Politechnika Warszawska, Warszawa (1981).
[175] D. Czyżewska, Rozprawa doktorska, Politechnika Warszawska, Warszawa (1988).
[176] V. G. Barylov, V. S. Demidov, A. N. Nikitenko *et al.*, Preprint ITEP-181, ITEP, Moscow (1984) [in Russian].
[177] C. W. Fabjan and R. Wigmans, Rep. Prog. Phys. **52**, 1519 (1989).
[178] A. I. Sessoms, M. S. Goodman, L. Holcomb *et al.*, Nucl. Instrum. Methods **161**, 371 (1979).
[179] T. A. Gabriel, B. L. Bishop, M. S. Goodman *et al.*, Nucl. Instrum. Methods **195**, 461 (1982).
[180] D. Fox, J. Simon-Gillo, M. W. Rawool-Sullivan *et al.*, Nucl. Instrum. Methods A **317**, 474 (1992).
[181] B. Słowiński and J. Rogulski, JINR Rapid Communications No. 4[55]-92, 19 (1992).
[182] F. Binon, V. M. Buyanov, M. Guaner *et al.*, Preprint IHEP-85-62, IHEP, Serpukhov (1985) [in Russian].
[183] DELPHI, Technical Proposal, DELPHI 83-66/1, CERN/LEPC/83-3 (1983).

Translated by Patricia A. Millard